Report No.
ATN-64(9227)-1

GENERAL RESEARCH

An Experimental Study of Secondary Flow in Jet-Driven Vortex Chambers

Prepared by

D. H. Ross,
Aerodynamics and Propulsion Research Laboratory

AEROSPACE CORPORATION
El Segundo, California

27 January 1964

Prepared for

VICE PRESIDENT AND GENERAL MANAGER
LABORATORY OPERATIONS

ABSTRACT

The characteristics of vortex flows in enclosed chambers are strongly influenced by the existence of three-dimensional secondary flows in the end-wall boundary layers and in a region near the axis. Classical "line-vortex" or two-dimensional treatments fail to account for these effects and no theoretical treatment to date has been able to account for all of the complicated interactions.

A series of flow visualization experiments was conducted to obtain a qualitative picture of the flow and the effects of changes in geometry and flow parameters. A transparent vortex chamber and selective dye injection into the water-working fluid were utilized. Interest centered on changes in the surface and shape of the end walls and on the exit hole. A form of end-wall-boundary-layer slot blowing was effective in altering the secondary flow pattern.

An approximate analysis is made to determine the effect of non-planar end-walls on boundary layer radial mass flow, based on the G. I. Taylor result for a conical swirl flow.

CONTENTS

FIGURES

FIGURES (Continued)

I. INTRODUCTION

Studies of viscous rotating or vortex flows have a long history. In the past 15 years an increase of both theoretical and experimental investigations has occurred, inspired largely by such applications as meteorology, Ranque-Hilsch tubes, cyclone separators, and gaseous vortex nuclear reactors (which provided the stimulus for the program reported herein).

Theoretical analyses of viscous vortex flows to date have not provided an adequate description of the complicated interactions present when the flow is bounded by solid surfaces at both the end and periphery. Boundary layers and secondary flow over the end walls are present and, in addition, annular zones of strong axial flow are observed. The experimental program discussed in this report was initiated to provide insight into the mechanism of the interaction problem and, thus, to aid future analysis.

Secondary flow in the end-wall boundary layers results from the tangential momentum defect in the boundary layer and the radially inward pressure gradient produced by the outer vortex flow. Outside the boundary layer the pressure gradient and the velocity field centrifugal force are in equilibrium. Within the boundary layer a net radial force acts upon the fluid; this force is the result of an undiminished pressure gradient and reduced centrifugal force when compared with the outer flow (Fig. 1).

Taylor[1] (1950) analyzed the secondary flow in the boundary layer on a converging conical surface with swirl flow, assuming laminar flow. He pointed out the large mass flow carried by this boundary layer. Weber[2] (1956) essentially repeated the Taylor analysis for laminar flow and obtained a related result for turbulent flow by making assumptions about the turbulent shear and velocity profiles. Rott[3] (1962) treated the turbulent case for flat end-walls from a different standpoint, but he also found the large radial boundary layer mass flow effect.

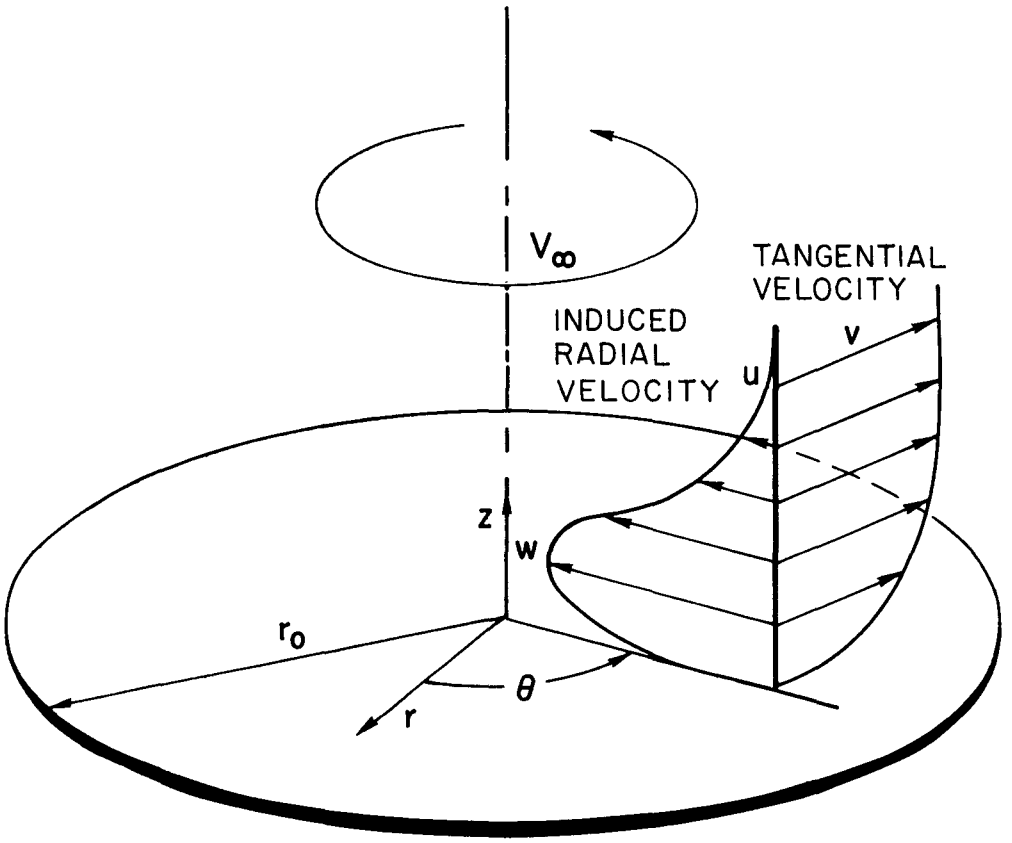

Fig. 1. Boundary Layer Flow Created by a Vortex Flow Over the Chamber End Wall

Kendall[4] (1962) made an experimental study of enclosed vortex flow which included observations of the end-wall boundary layers and velocity traverses of the layers. He also discussed applicability of previous three-dimensional boundary layer analyses to the end-wall case.

The frequently observed concentric zones of secondary flow near the axis are the result of a complicated coupling between the main vortex flow, the end-wall boundary layers, and the pressure field set up by the passage of fluid out the exit hole (see Figs. 11, 12, 13). Kendall (1962) observed and discussed such zones in addition to the work on the end wall boundary layer. Rosenzweig, Ross and Lewellen[5] (1962) report on observations of this phenomenon in a vortex flow visualization apparatus and discuss some of the flow details. This last reference is based upon the earliest part of the experimental program described in this report. Similar phenomena have been reported by Binnie and Teare[6] (1956) for swirling flow in a conical chamber; Smith[7] (1961) for a cylindrical cyclone separator with the vortex flow driven at one end, that through which the flow exited from the chamber; and Thompson[8] (1963) for a configuration similar to that of Smith aside from the placement of the flow inlet and exit at opposite ends of the chamber.

Theoretical treatment of viscous vortex flow has only recently included enough of the complications present when the flow is enclosed by solid boundaries to be of value in this case. Boundary conditions fixed at infinite radius, or arbitrary assumptions about the three-dimensional character, commonly limit the applicability of the earliest work. Lewellen[9] (1962) presents a three-dimensional solution which is not restricted along these lines; in fact, if independent knowledge is available to specify the proper boundary conditions at the vortex periphery and exit hole, this analysis could be applied to predict the flow field in the strong circulation case. His paper also contains a critical review of previous theoretical investigations. The report of Rosenzweig, Lewellen and Ross[10] (1964) attempts to analyze a case which approaches the complexity of the real physical situation. The

interaction between the interior vortex flow and the end-wall boundary layers is explicitly treated by coupling the equations resulting from the analysis of the vortex flow by Lewellen[9] (1962) and that of the end-wall boundary layer by Rott[3] (1962).

The experiments and observations described in this report were the experimental complement to the analytical work in vortex flow conducted at Aerospace Corporation, part of which was mentioned in the foregoing paragraph. Study of the boundary layer and secondary flow regions was facilitated by the selective injection of colored dye within a transparent vortex chamber as described below.

II. EXPERIMENTAL APPARATUS

The basic apparatus is shown in Figs. 2 and 3. The flow chamber proper is the region bounded by the inner lucite cylinder and the flat lucite end walls. The space between the inner and outer cylinders forms a plenum chamber to feed the two rows of fine, closely spaced holes in the wall of the inner cylinder. The holes are tangent to a circle of radius slightly less than that of the inner surface and the resultant jet flow imparts angular momentum to the fluid within the chamber (see Fig. 4). One or both of the end walls contains an exit hole at the center.

The plenum is supplied with water from a centrifugal pump at pressures up to 60 psig. Flow rate and pressure level are controlled independently by means of throttle valves both upstream of and downstream from the chamber (Fig. 3).

A dye injection probe injects tracer fluid almost tangentially from the end of a fine hypodermic tube. The latter is connected to a pressurized supply of dye through the hollow probe stem. The probe stem can be traversed

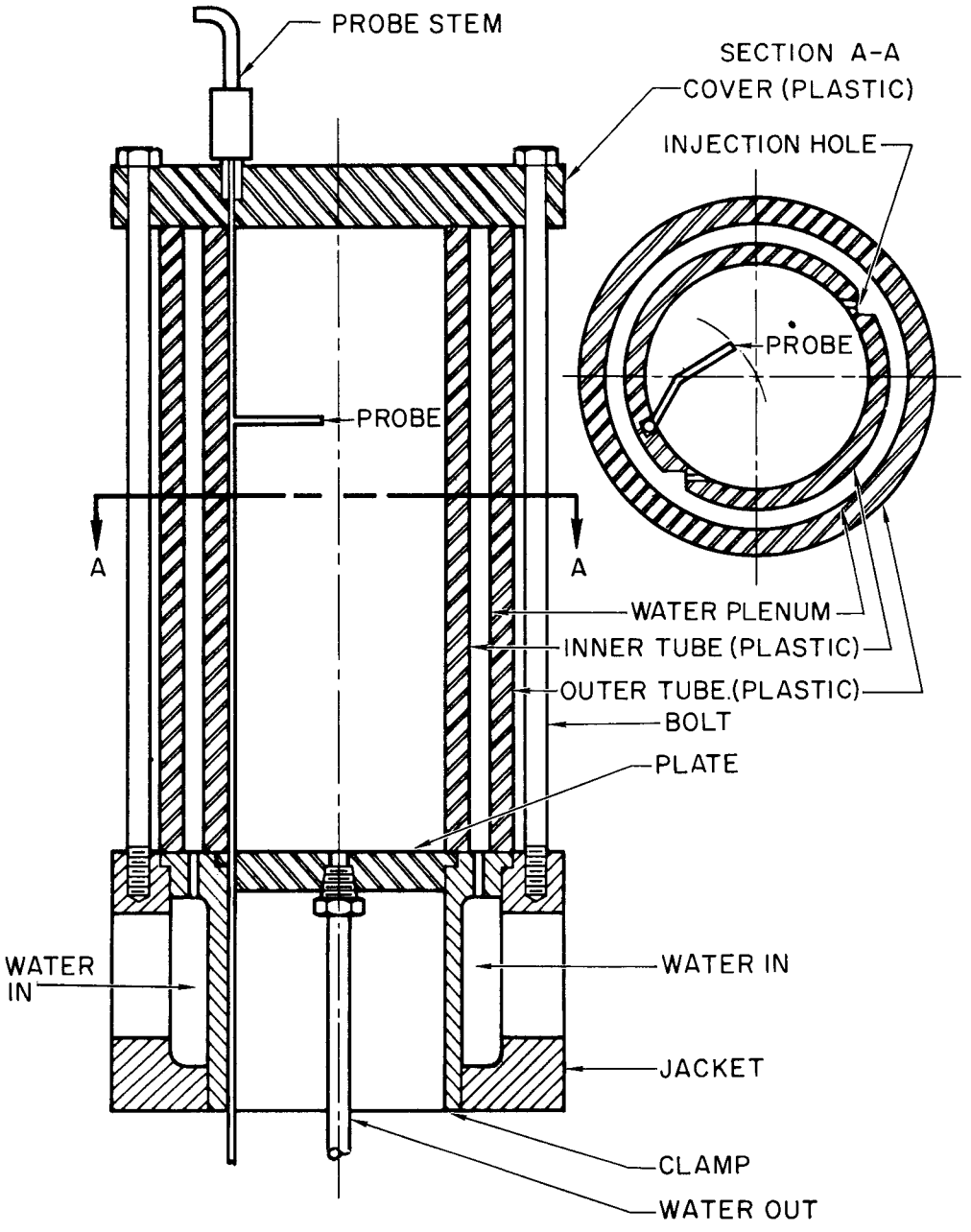

Fig. 2. Diagram of Flow Visualization Apparatus

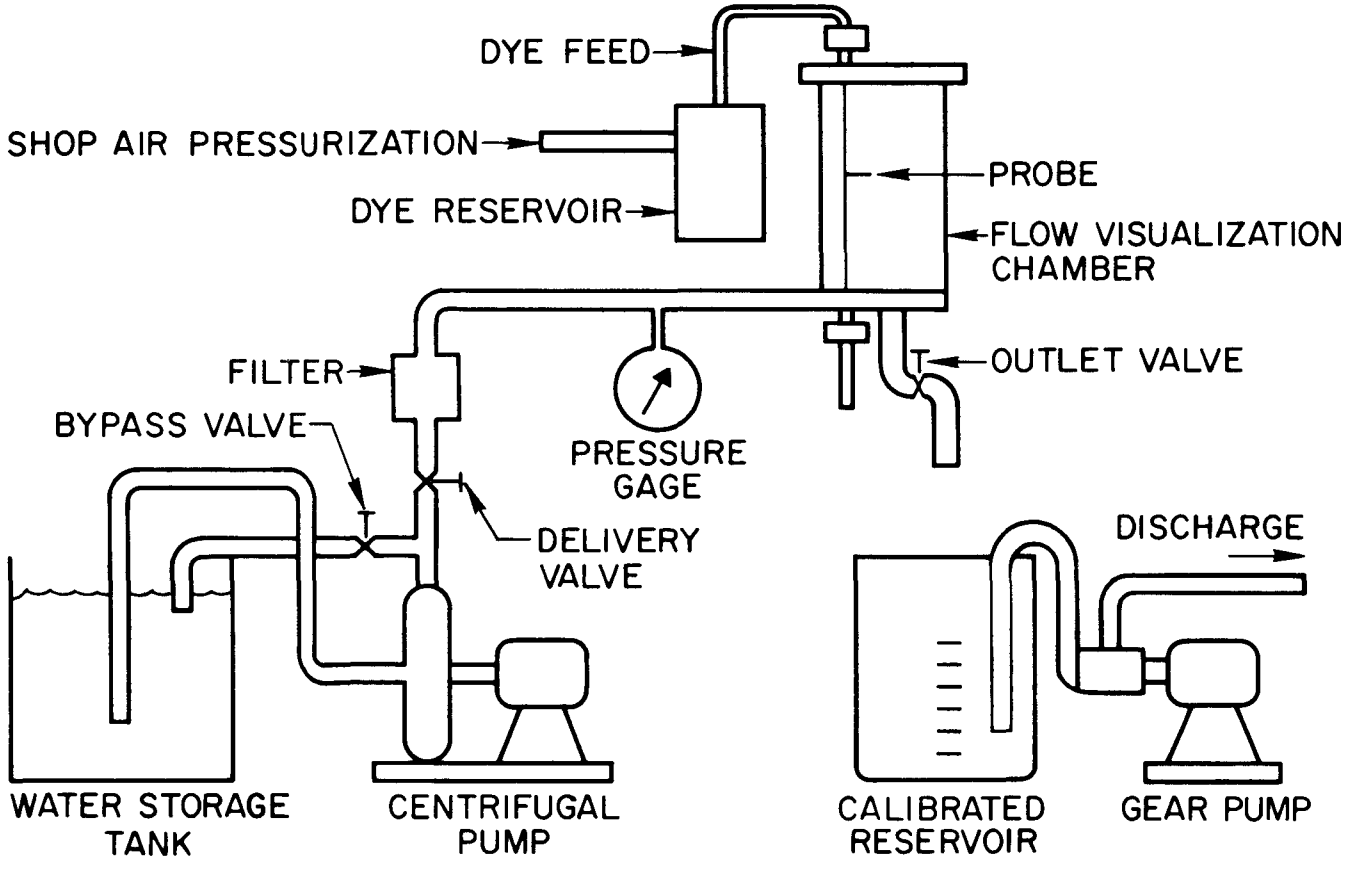

Fig. 3. Diagram of Flow Visualization System

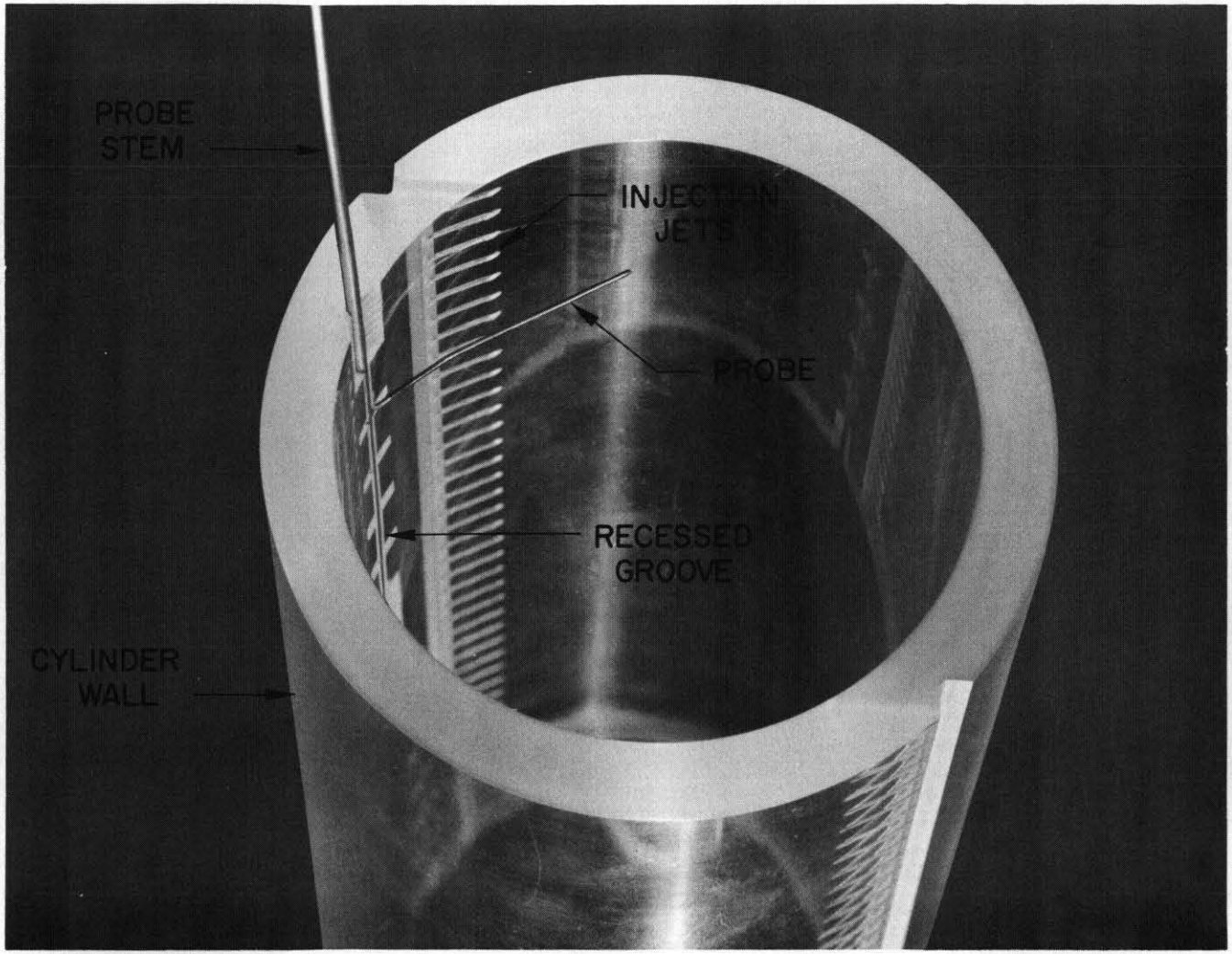

Fig. 4. Vortex Chamber Inner Cylinder

axially and rotated so that dye can be discharged at desired points in the flow chamber. The stem is contained within a recessed groove to minimize disturbance to the vortex flow. The probe is also shown in Fig. 4. The dye injection chamber is illustrated in Fig. 5.

The basic apparatus can be altered by replacing the inner cylinder with another one which has different injection geometry, and by replacing end walls with other walls which have different shapes or exit hole sizes. An injection geometry was selected which gave a reasonably narrow jet mixing region near the wall without undue constructional difficulty (see Figs. 2 and 4). Several types of probes were developed to give minimum disturbance to selected portions of the flow field.

A variety of end-walls was tested in an attempt to influence the secondary flow zones. Figure 6 shows a sample of the end-wall configurations used in the program. Exit-hole-to-cylinder diameter ratios of 0.023 to 0.354 were employed. Most examples had a sharp-edged exit hole, however, selected sizes had rounded edges or inward projecting lips. In addition, the results with slightly conical smooth and ringed surface ends were compared with their flat counterparts. Surface variations also included abrasive paper and small vertical wire "vortex generators" similar to the devices used to delay separation from airfoil surfaces.

End-wall slot blowing involved major modification of the apparatus. Two separately fed end-wall plenum chambers having four radial slots were substituted for the usual upper and lower end walls. Figure 7 shows the upper and lower units. A later version utilized lucite plates with narrower slots and had four additional partial radius slots at the outer periphery for improved performance. Additional valves and piping allowed the mass flow to be divided between the side and end plenum chambers, two flow meters being used to determine the respective amounts. An additional dye chamber allowed introduction of dye into the end wall feed to follow the path of the

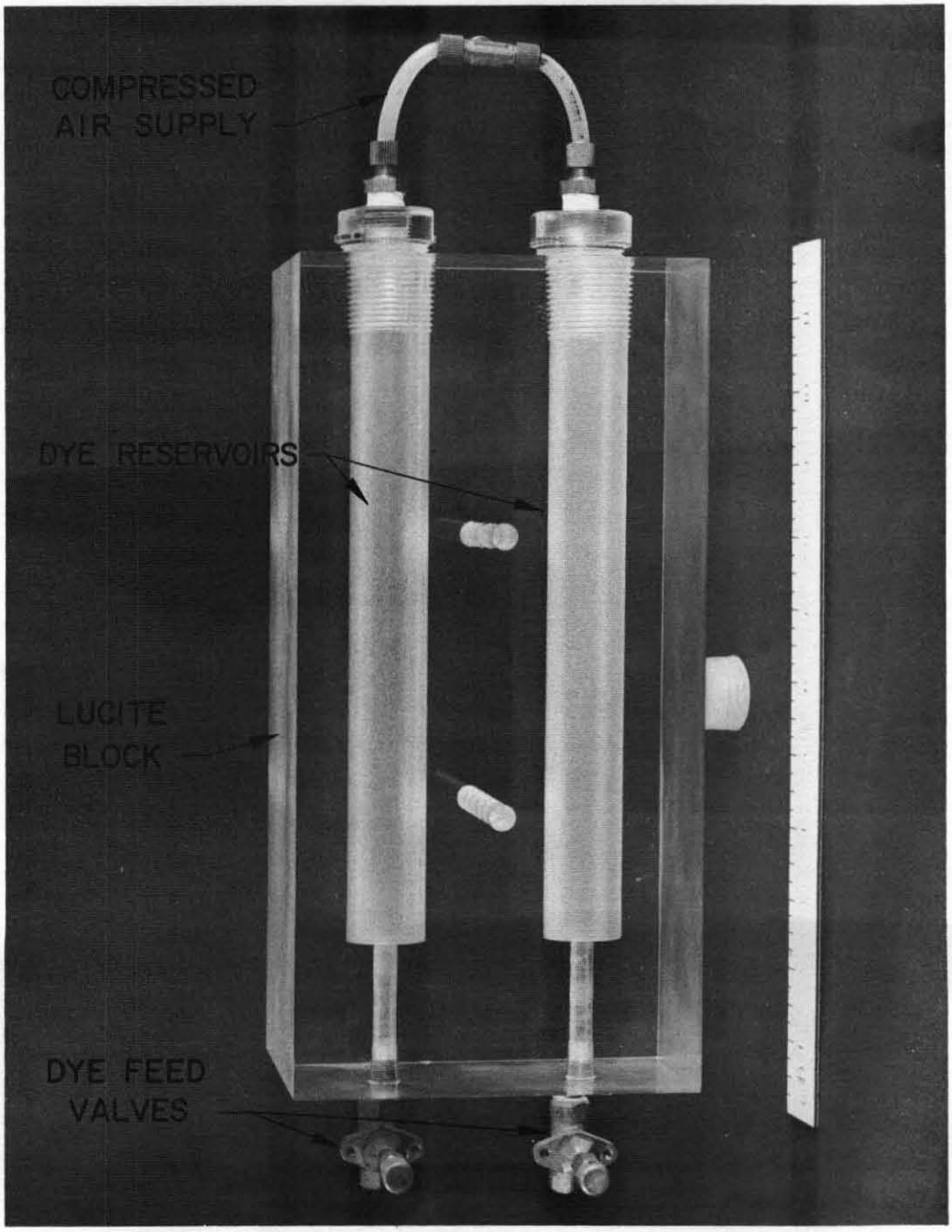

Fig. 5. Dye Chamber

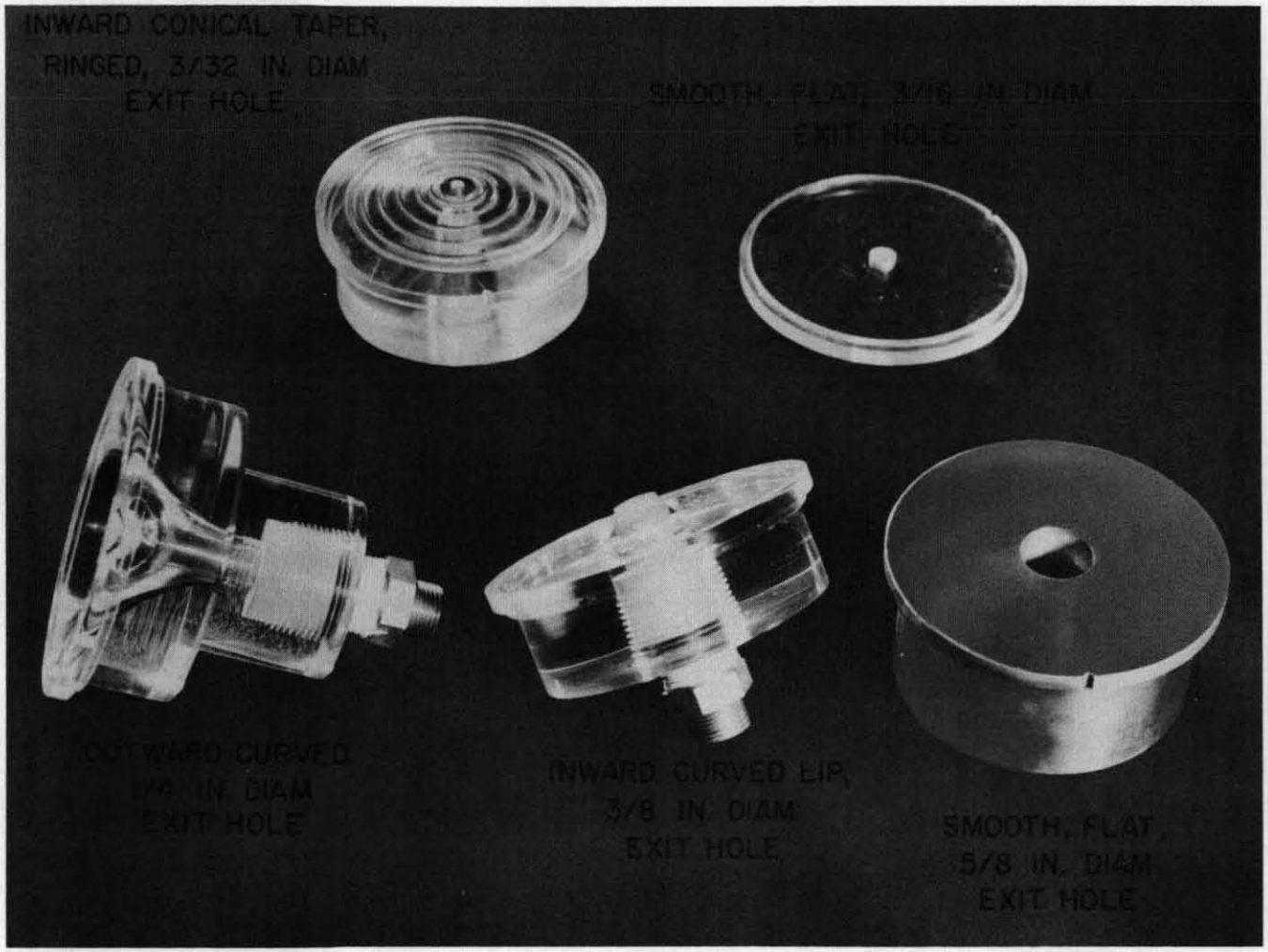

Fig. 6. Sample of End Walls Tested

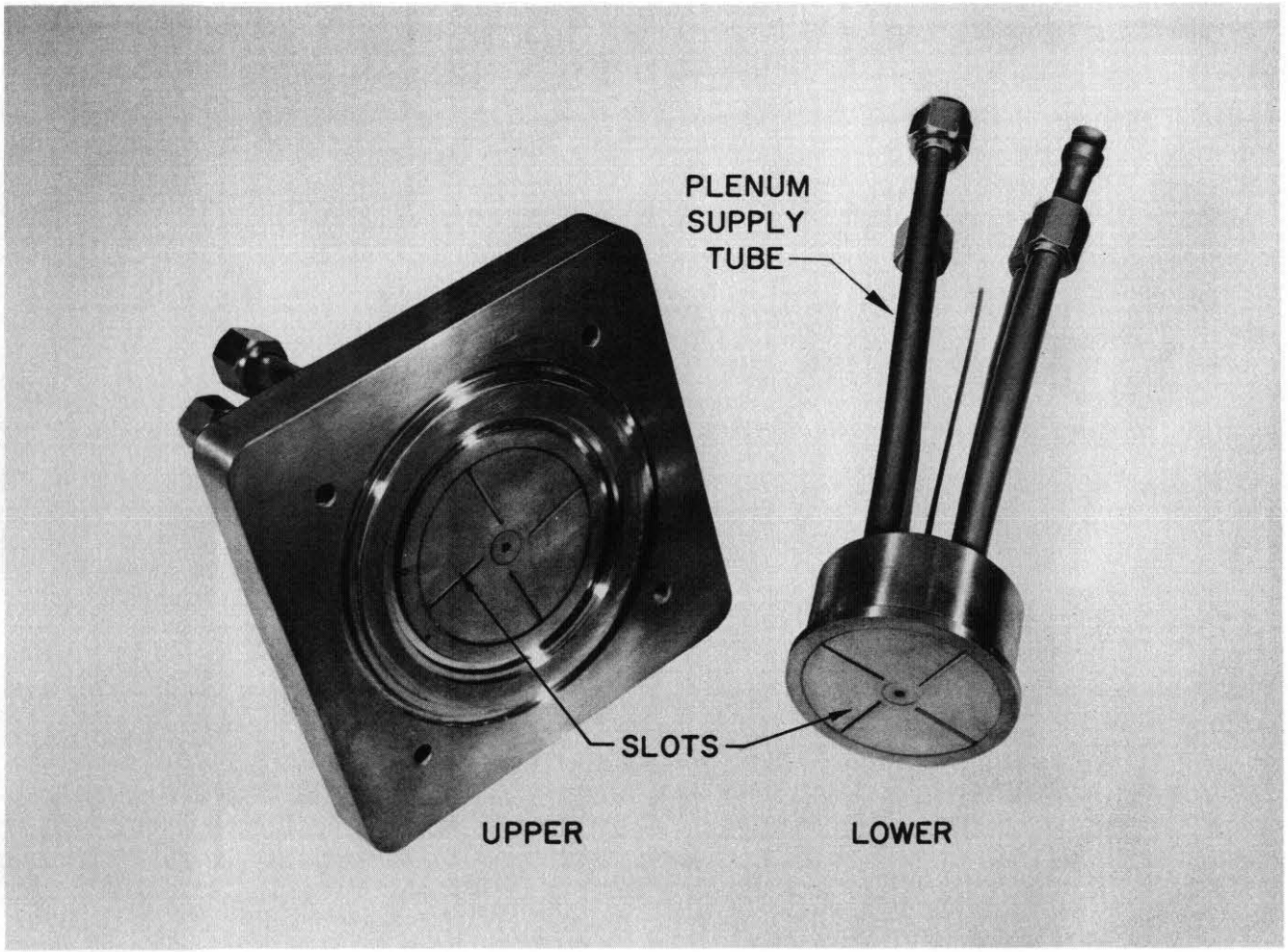

Fig. 7. End Walls for Slot Blowing

slot-blowing fluid. The main part of this system is shown in Fig. 8, and a drawing of the end wall assembly showing details of both versions of slot is presented in Fig. 9.

III. PROCEDURE

The basic method of operation was to inject dye into a selected portion of the flow field and observe the short time paths of the tracer fluid. Visual observation was aided by both still and motion picture photography; color and black-and-white films were used.

Because water was the only vortex working fluid employed, the dyes were of the organic water-soluble variety. Methyl Violet, Methylene Blue, Acid Chrome Blue and Nigrosine Black gave the best results under strong incident visible-light illumination. As strong concentrations raised the specific gravity of the dye fluid, a small amount of alcohol was added to reduce the specific gravity to equal that of the working fluid. The value was measured by a precision hydrometer. The extremely high centrifugal force field in the vortex flow stimulated this precaution.

A later refinement was the use of a Fluorescein dye solution and long wave UV illumination. When illuminated by four standard 15-in. "black light" tubes and viewed through yellow glasses, it was possible to distinguish details of the flow readily with extremely low dye concentrations. This low concentration also minimized distortion of the observed patterns by the phenomenon of concentration gradient diffusion. Color motion picture photography was possible with high speed film and appropriate filters. An additional benefit accruing from the low concentrations required was the elimination of the need for specific gravity balancing.

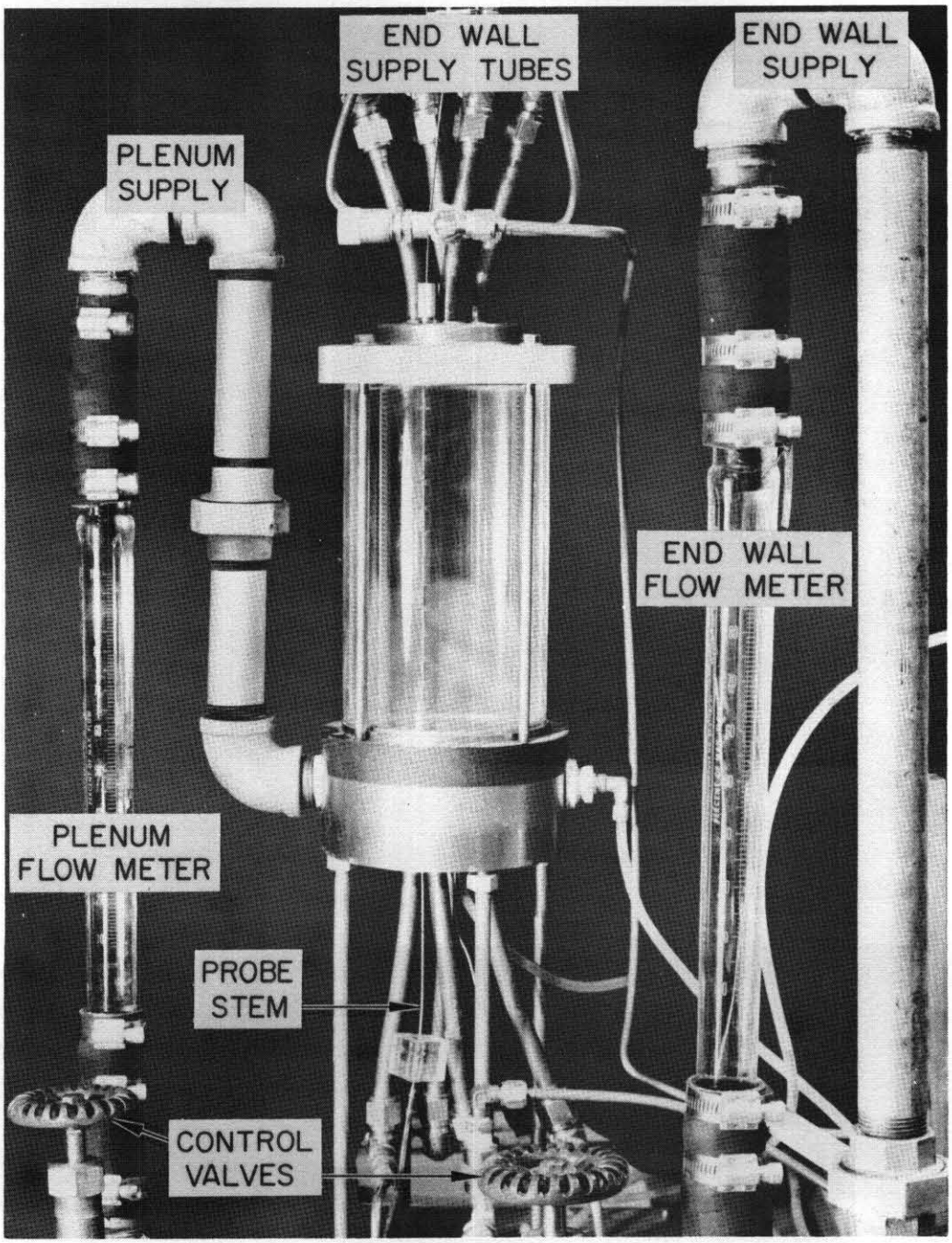

Fig. 8. Overall View of the Flow Visualization Apparatus Equipped for End Wall Injection

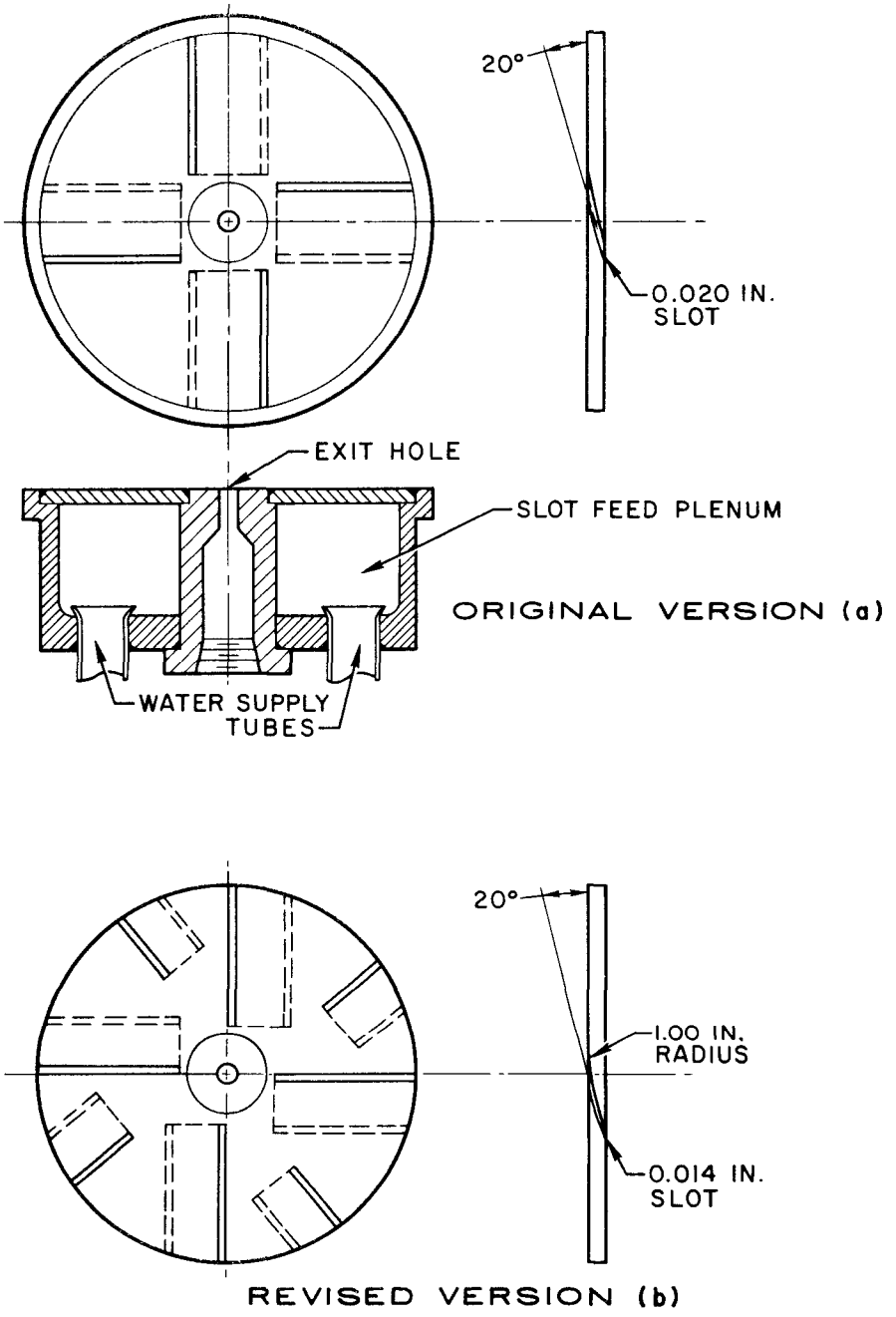

Fig. 9. Lower End Wall Slot Blowing Configuration

The maximum mass flow attainable depended upon the exit-hole diameter and provision for single or double ended exhaust. The maximum volume flow was normally from one to two gal/min. This flow corresponded to an average radial Reynolds number of 70 to 150 (where $Re_r = \rho Q/2\pi L\mu$). The flow could be reduced to a radial Reynolds number of 2; the flow was then apparently laminar as evidenced by the long wirelike spiral dye streams (Fig. 10). Most intensive investigation was conducted in the range of Reynolds numbers from 40 to 100.

When the slot-blowing end walls were installed, the behavior of the central core and end-wall boundary layer regions were observed by means of the Fluorescein dye - UV light technique. Usual procedure was to vary the percentage of the total vortex mass flow injected through the end-wall slots from 0 to 100 percent, continuously or in discrete steps. Total flow (composed of end-wall plus sidewall injection fractions) was held constant during these experiments. In addition to the usual probe injection, dye could be introduced to upper and lower plenum chambers by a separate feed system, resulting in dyed slot-blowing fluid which aided identification of the flow pattern in the vicinity of end wall.

IV. OBSERVATIONS AND RESULTS

The main objective in this program was to observe the flow patterns within the vortex chamber, with emphasis upon the shear interaction regions where substantial departures from simple vortex theory could be expected. These regions were the end-wall boundary layer and the central portion of the chamber where strong axial secondary flow occurred. Mass flow was varied and exit holes altered in an attempt to discover if these changes influenced the flow characteristics.

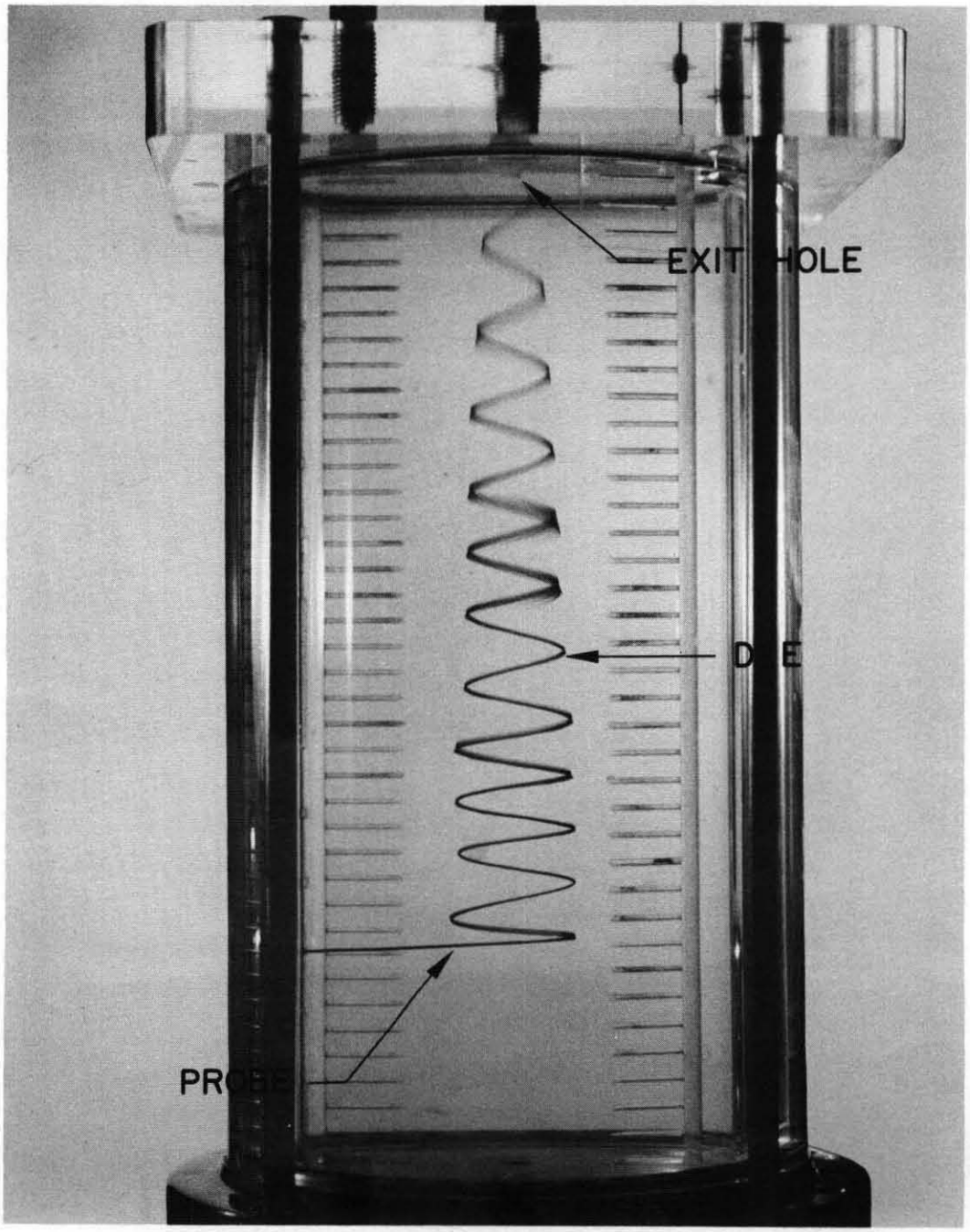

Fig. 10. Flow Visualization Chamber Showing Dye Filament at Low Reynolds Number

Initial work with dark colored dyes in a simple configuration having plane end walls with a 1/8-in. diameter hole established the existence of a multiple-zone region of axial secondary flow near the axis of the vortex. This zone is a persistent feature of the flow for a wide range of conditions including variations in mass flow and configuration.

This axial-flow core is shown in Figs. 11 and 12. A diagram of the structure of such a flow is shown in Fig. 13 which represents the result of numerous visual observations, motion picture studies, and still photos. The exit hole is in the bottom end wall. The essential features of the core are a strong axial downflow region (A) from the upper end wall boundary layer to the exit hole in the lower end wall, the diameter of (A) is approximately equal to the exit hole diameter; an annular upflow region (B) surrounding (A); and somewhat diffuse downflow region (C) outside of (B). A detailed discussion of this phenomenon and a hypothesis for the interactions involved was given by Rosenzweig, Ross and Lewellen[5] (1962) and Rosenzweig, Lewellen and Ross[10] (1964).

Reference 5 was based upon the first portions of the program reported herein. Subsequent experimental work was directed toward investigation of the core structure and attempts to alter the pattern by changes in the chamber configuration. Reference 10 was influenced by the results of these studies.

Figures 14 through 18 demonstrate the similarity in flow pattern for a series of varying-radius end walls. The mass flow rate in each case is similar. Figure 14 was made with a 1/16-in. diameter sharp-corner exit hole, Fig. 15 with a 1/8-in. diameter slightly-rounded-corner hole, Fig. 16 with a 1/8-in. diameter hole having a 1/4-in. radius rounded-entrance section, Fig. 17 a 3/16-in. diameter sharp-corner hole, and Fig. 18 was made with the 5/8-in. diameter sharp-corner hole. The same basic pattern can be discerned in all cases and only in the case of the 5/8-in. diameter hole is

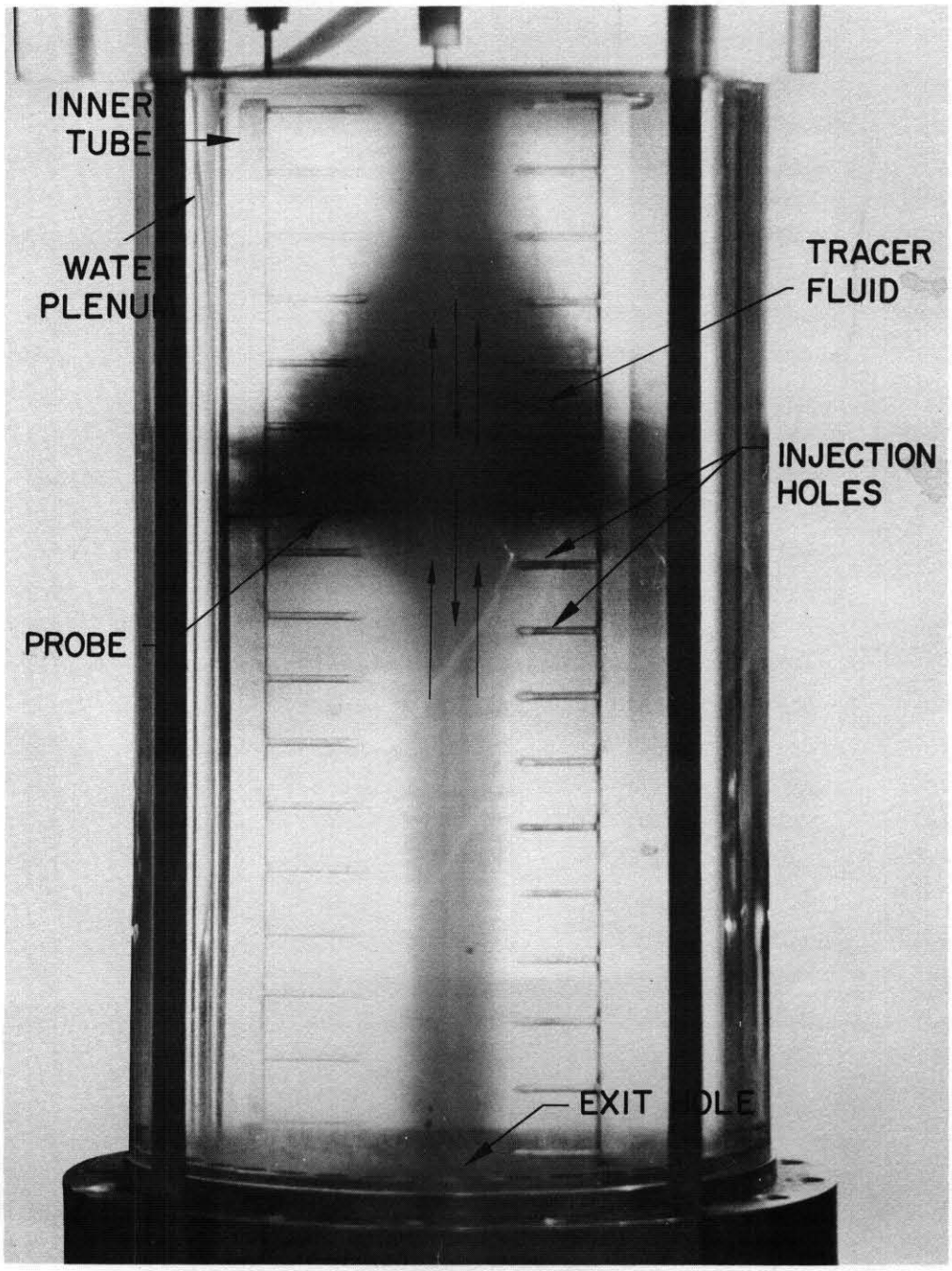

Fig. 11. Flow Visualization Chamber Showing Tracer Fluid Injected near Side Wall

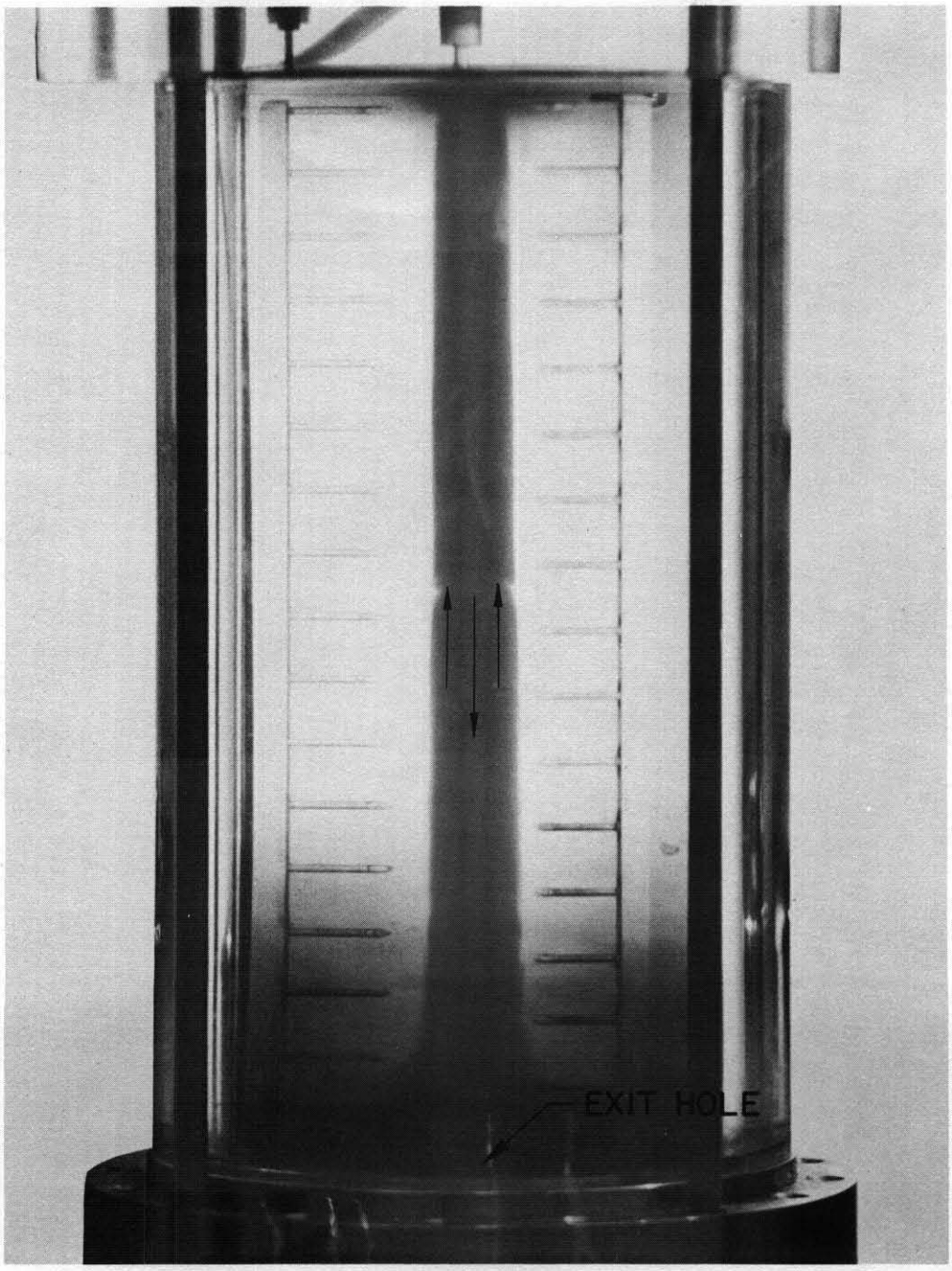

Fig. 12. Flow Visualization Chamber Showing Tracer Fluid Injected near Lower End Wall

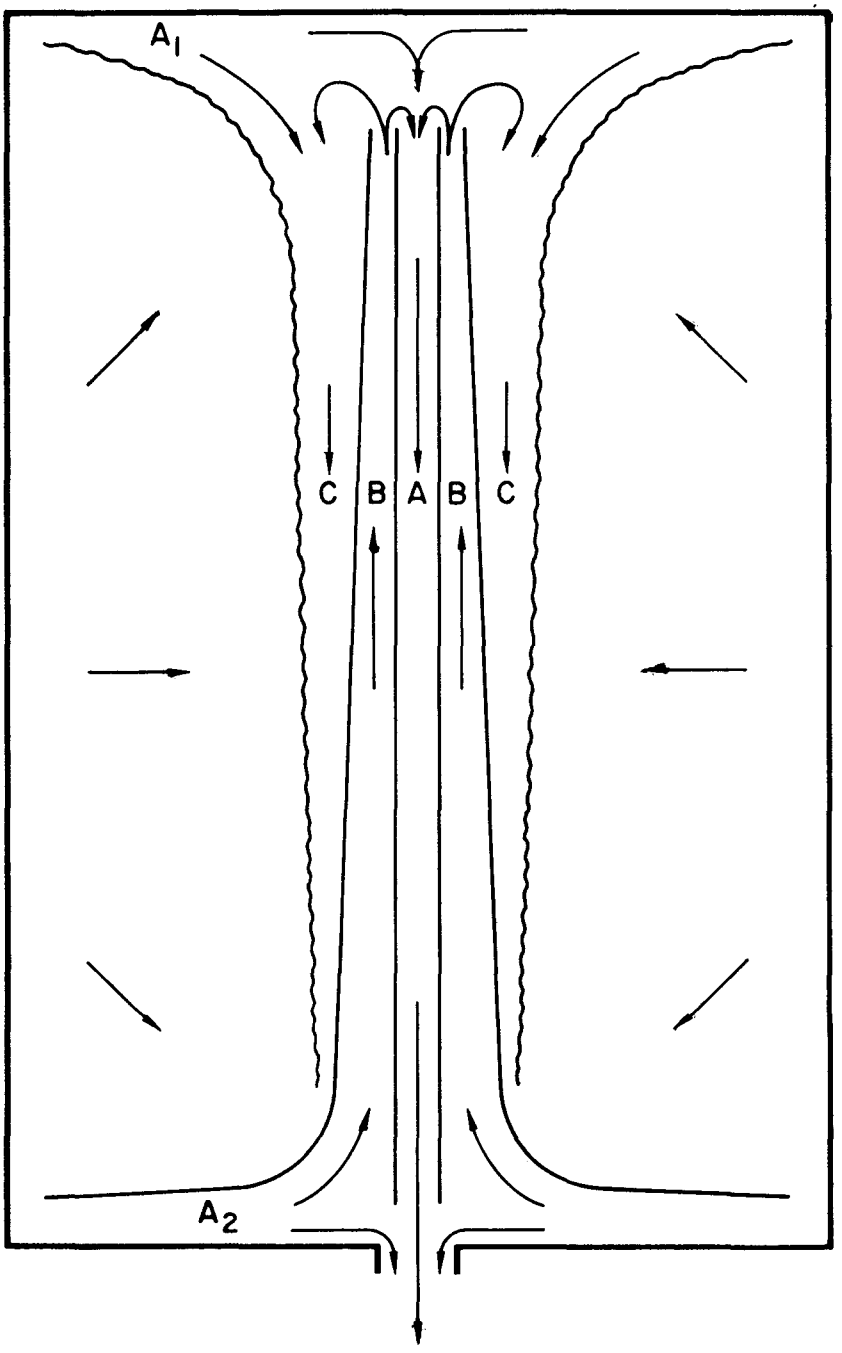

Fig. 13. Conceptual Diagram of Three Dimensional Flow in Vortex

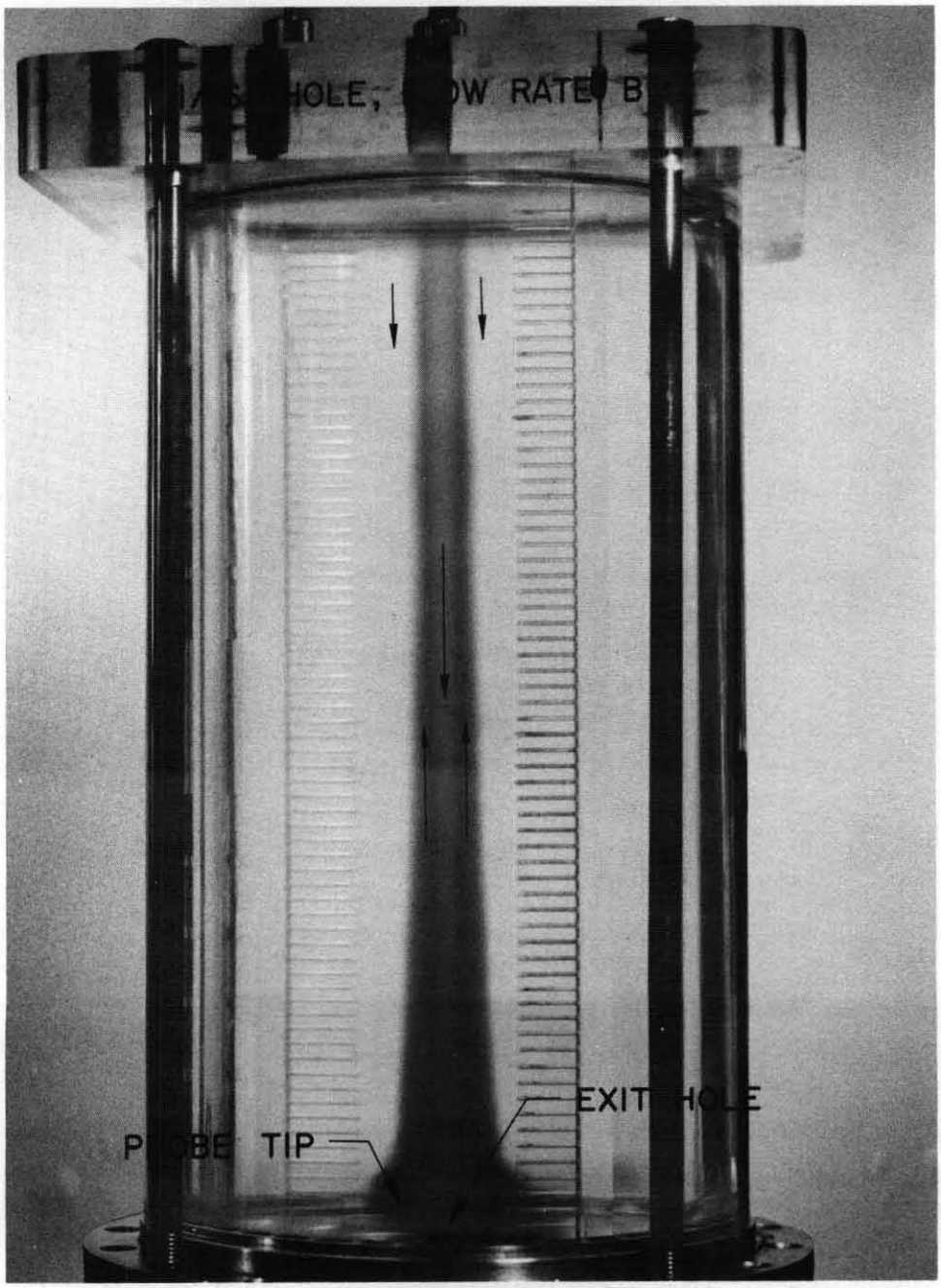

Fig. 14. Axial Flow Ejection from End Wall Boundary Layer. 1/16 Inch Diameter Exit Hole

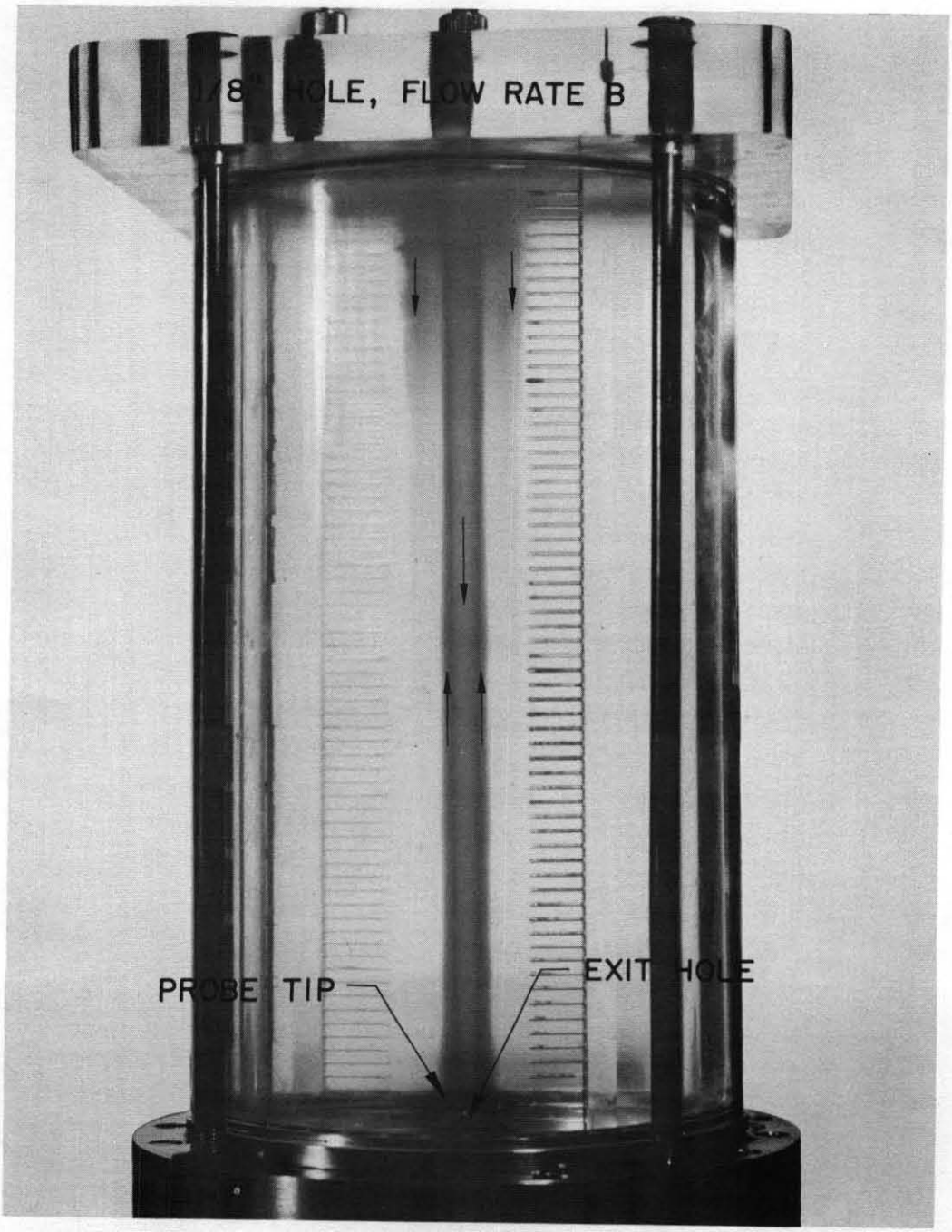

Fig. 15. Axial Flow Ejection from End Wall Boundary Layer. 1/8 Inch Diameter Exit Hole

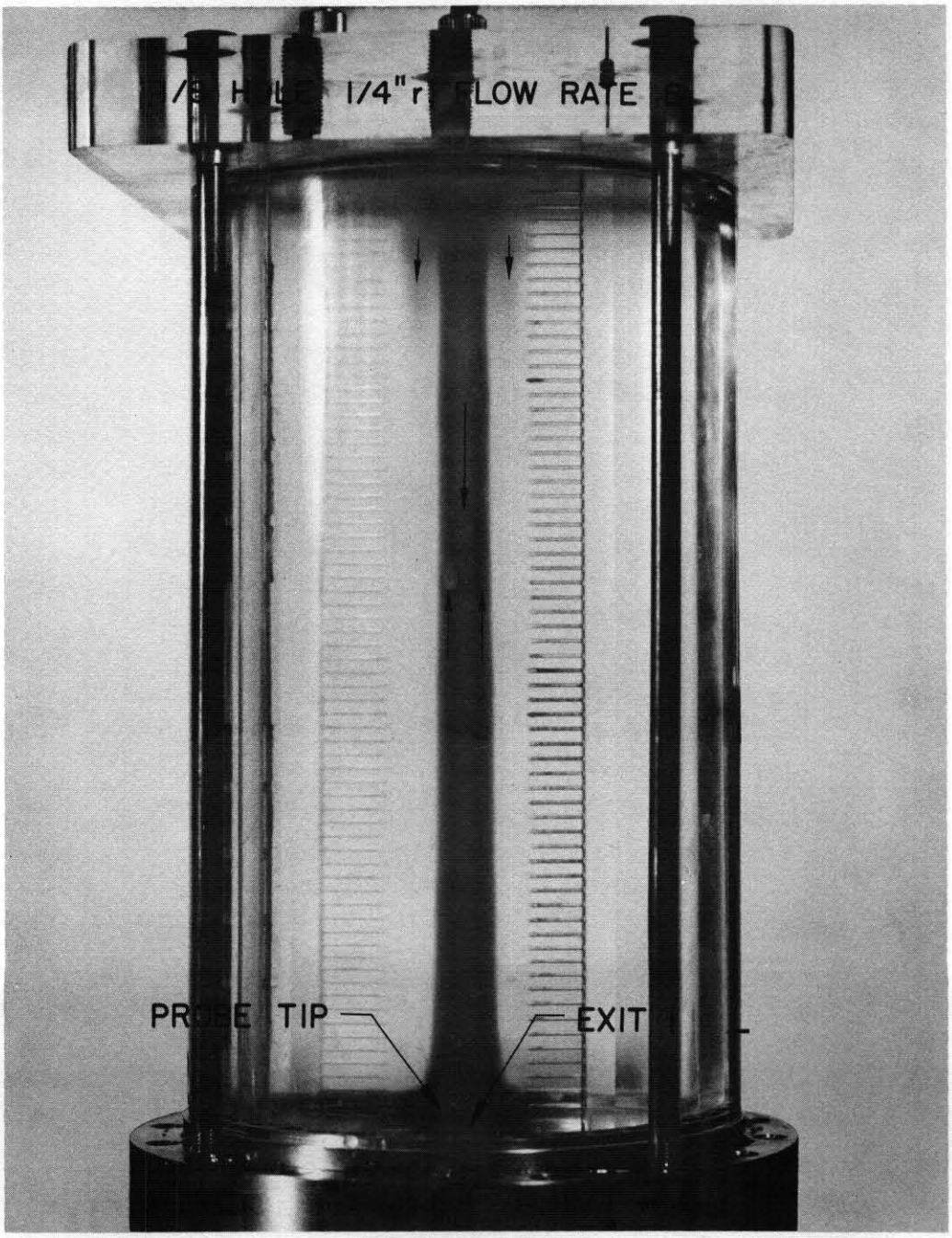

Fig. 16. Axial Flow Ejection from End Wall Boundary Layer.
1/8 Inch Diameter, 1/4 Inch Radius Entrance, Exit Hole

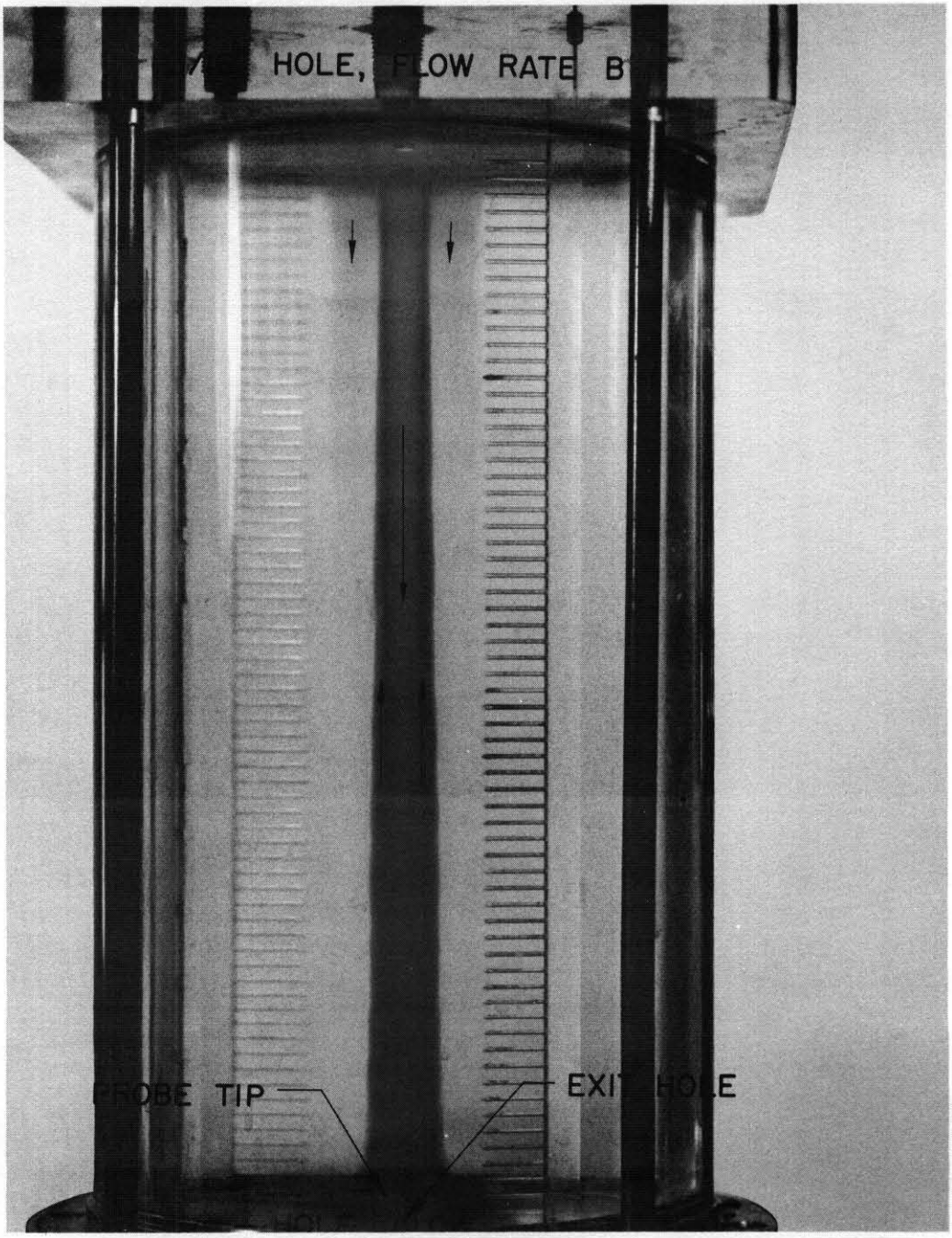

Fig. 17. Axial Flow Ejection from End Wall Boundary Layer.
3/16 Inch Diameter Exit Hole

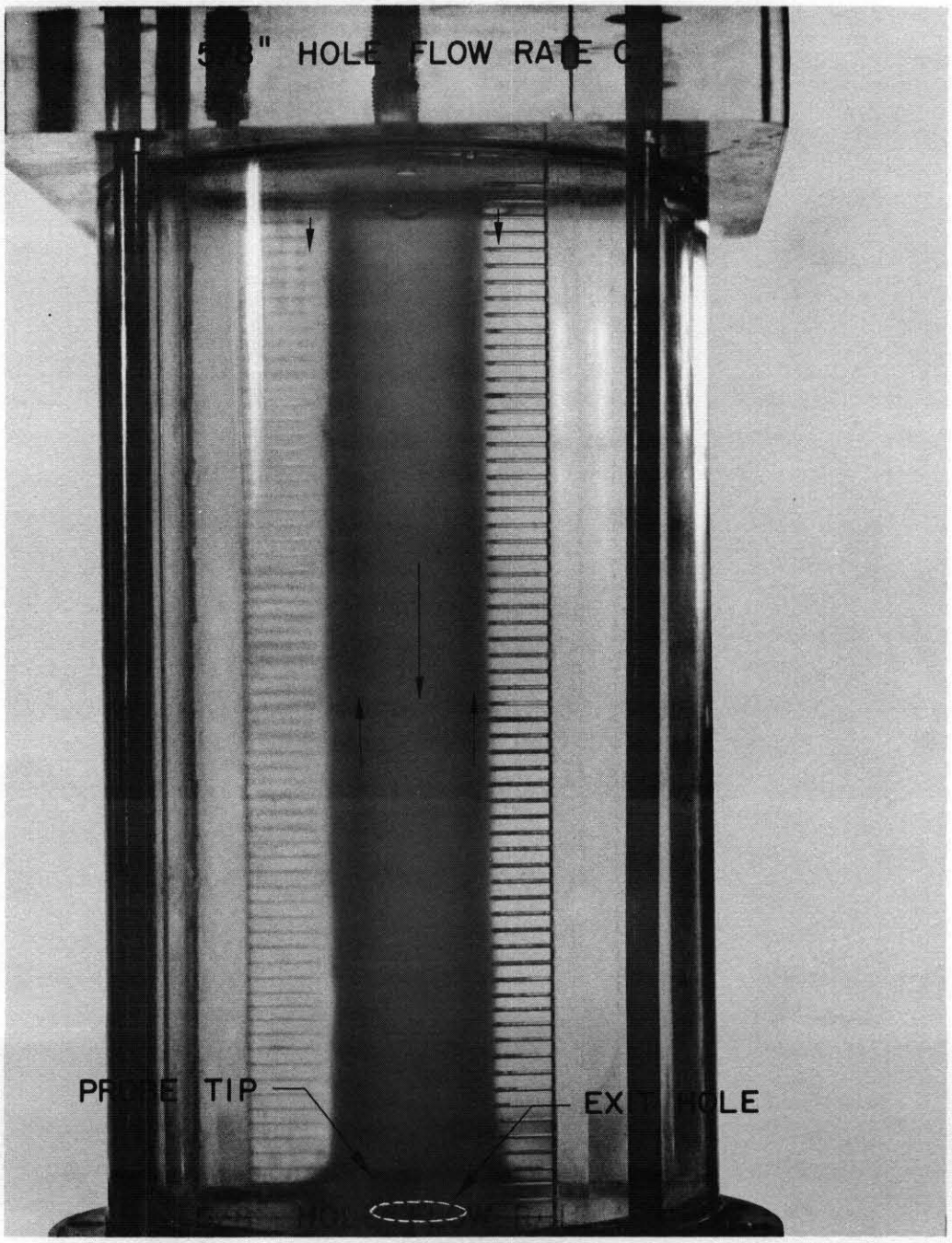

Fig. 18. Axial Flow Ejection from End Wall Boundary Layer. 5/8 Inch Diameter Exit Hole

a substantial change in the scale of the core flow noted. This previously described A, B, C zone core was always observed in a large number of tests covering an even wider range than the examples referred to above.

Studies of changes in the end-wall surface (including rings, abrasive, vortex generators, etc., some of which are illustrated in Fig. 6) produced the same general conclusions as above. The now familiar axial flow core was always a dominant feature of the flow, joined by new concentric zones of axial flow in those cases where the vertical scale of the protuberences was on the order of, or greater than, the boundary layer thickness. In the latter cases a strong interaction with the end-wall boundary layer produced a local mass flow rejection from the layer and a resultant annular region of axial flow.

One case which did produce a noteworthy new feature in addition to the usual central core structure was that of highly outward curved end walls, where the end wall surface had a radius nearly equal to that of the chamber, tangent to the horizontal at the wall and to the vertical at the exit hole thus forming a shape similar to the convergent portion of a rocket nozzle (shown at the lower left hand corner of Fig. 6). Figures 19 and 20 are photographs of this case taken with the aid of Fluorescein dye-UV technique. Figure 19 depicts a pulse of dye added at the surface of the side wall midway between the two end walls. The picture was obtained a few seconds after the introduction of the dye pulse. The bright large diameter collar in the middle of the chamber represents the trailing edge of the pulse and thus the location of the dye just after it emerges into the flow. The hazy column tapering inward and toward both ends shows the region occupied by the dye as it traverses the main part of the vortex flow. The sharp, nearly parallel bright areas represent the edges of a cylindrical region surrounding the A, B, C core. The latter core region is not noticeable in this photo due to the position and timing of the dye injection. The cylindrical region of strong dye concentration is formed very rapidly after dye injection and remains

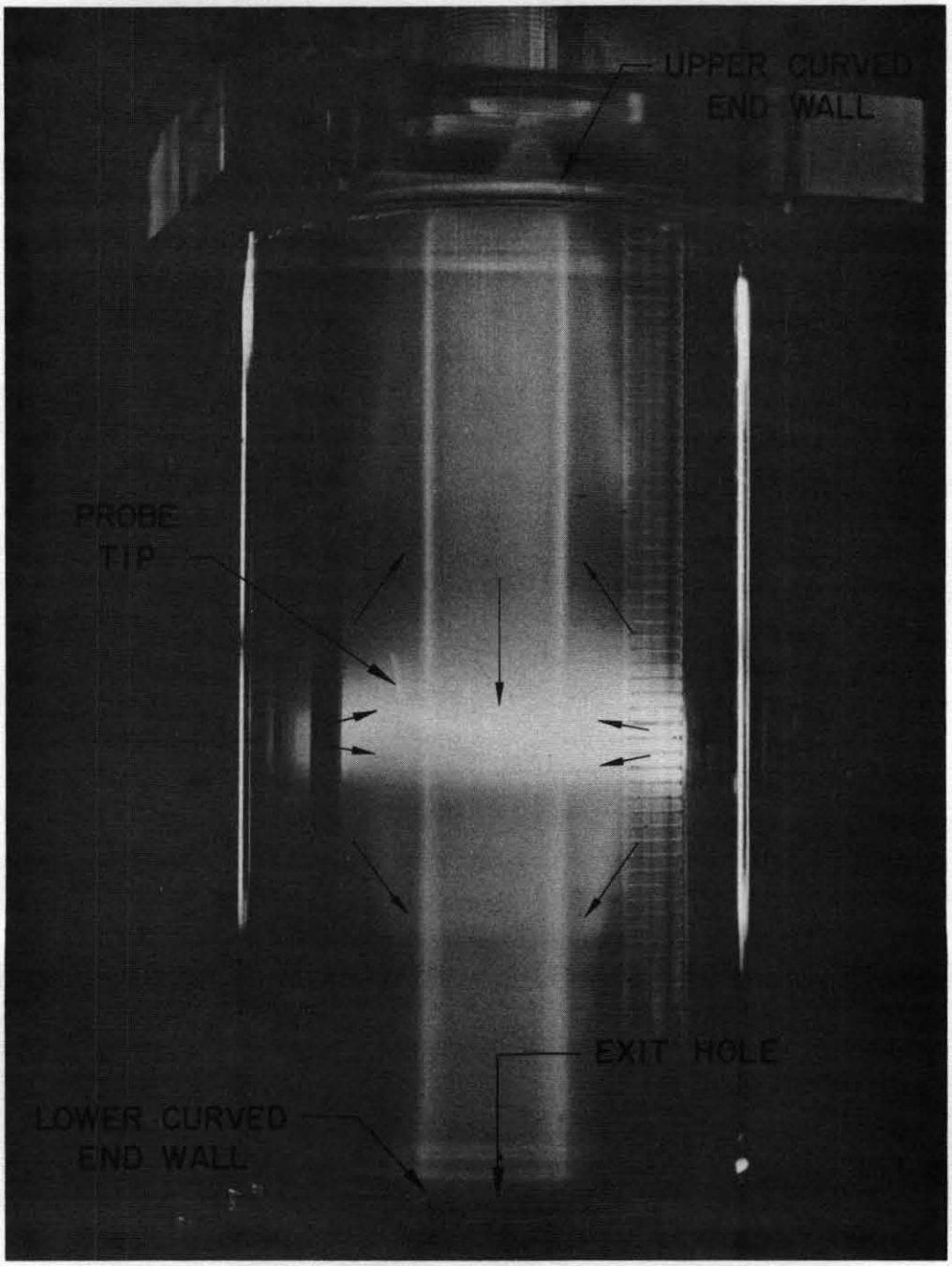

Fig. 19. Large Radius, Highly Curved End Wall. Photograph Taken at End of Initial Fluorescein Dye Pulse

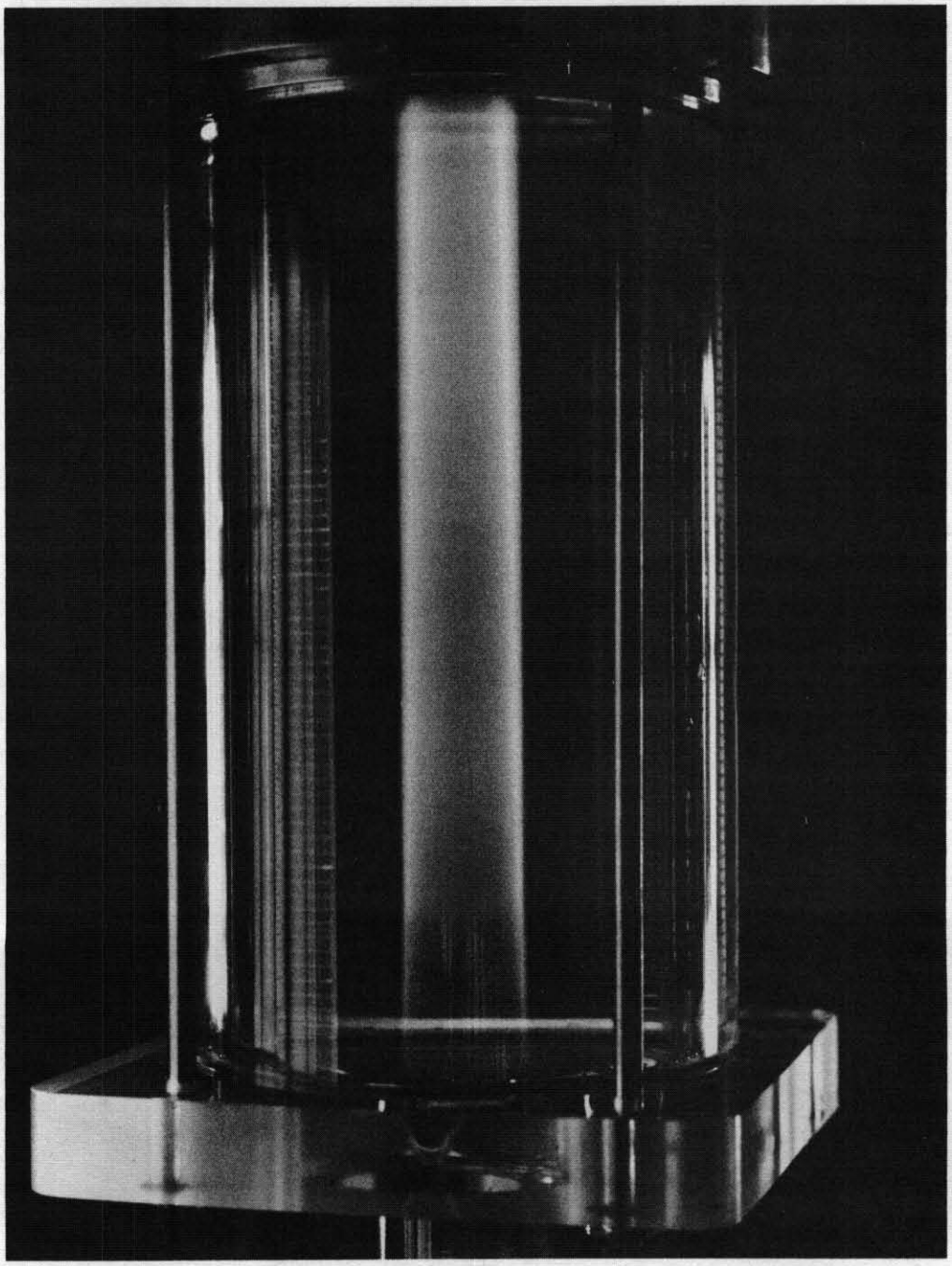

Fig. 20. Highly Curved End Wall. Stable Cylinder of Fluorescein Dye. Photograph Taken Approximately 10 Minutes after Initial Dye Input with Vortex Operating at Maximum Flow Rate

rather stable for a very long period. Figure 20 was taken several minutes after Fig. 19 and still shows a strong and persistent concentration of dye. A noticeable photographic image was obtained after 12 to 15 min. of high Reynolds number flow ($Re_r \doteq 150$) at 2 gal/min with an initial dye pulse of only a few cubic mm. The photographs were produced by internegative process from color film with an ASA rating of only 25.

This annular zone of dye "containment" indicates a simultaneous vanishing of axial and radial velocity components. The persistent zone is also an indication of laminar flow in this region since strong turbulent diffusion would result in quick dissipation. In Appendix A, it is shown that departure from flat end walls results in increased boundary layer mass flow due to the greater wall area contributing to fluid shear. It is hypothesized that the observed flow patterns for the highly curved end wall configuration result from a boundary layer mass flow which is greater than the injected mass flow. For steady-state continuity to be satisfied in this case, some sort of recirculation pattern must be postulated.

Application of the approximate three-dimensional boundary layer theories (such as that of Rott) to the flat-end-wall case for realistic values of the system parameters often results in a predicted boundary layer radial mass flow equal to or even greater than the injected flow. In such calculations the only input from the primary vortex flow field is the measured or assumed circulation distribution. Once the circulation distribution has been prescribed, the radial distribution of boundary-layer radial inflow has been fixed and the ratio of this to the total injected mass flow will be determined by the chamber length-to-diameter ratio and tangential Reynolds number (a uniform injected mass flow per unit length of chamber has been assumed).

It is interesting to note that the observed axial flow structure within the stable cylinder (Fig. 21) appears to be quite similar to the structure described previously for the flat-end-wall configuration. It is probable that

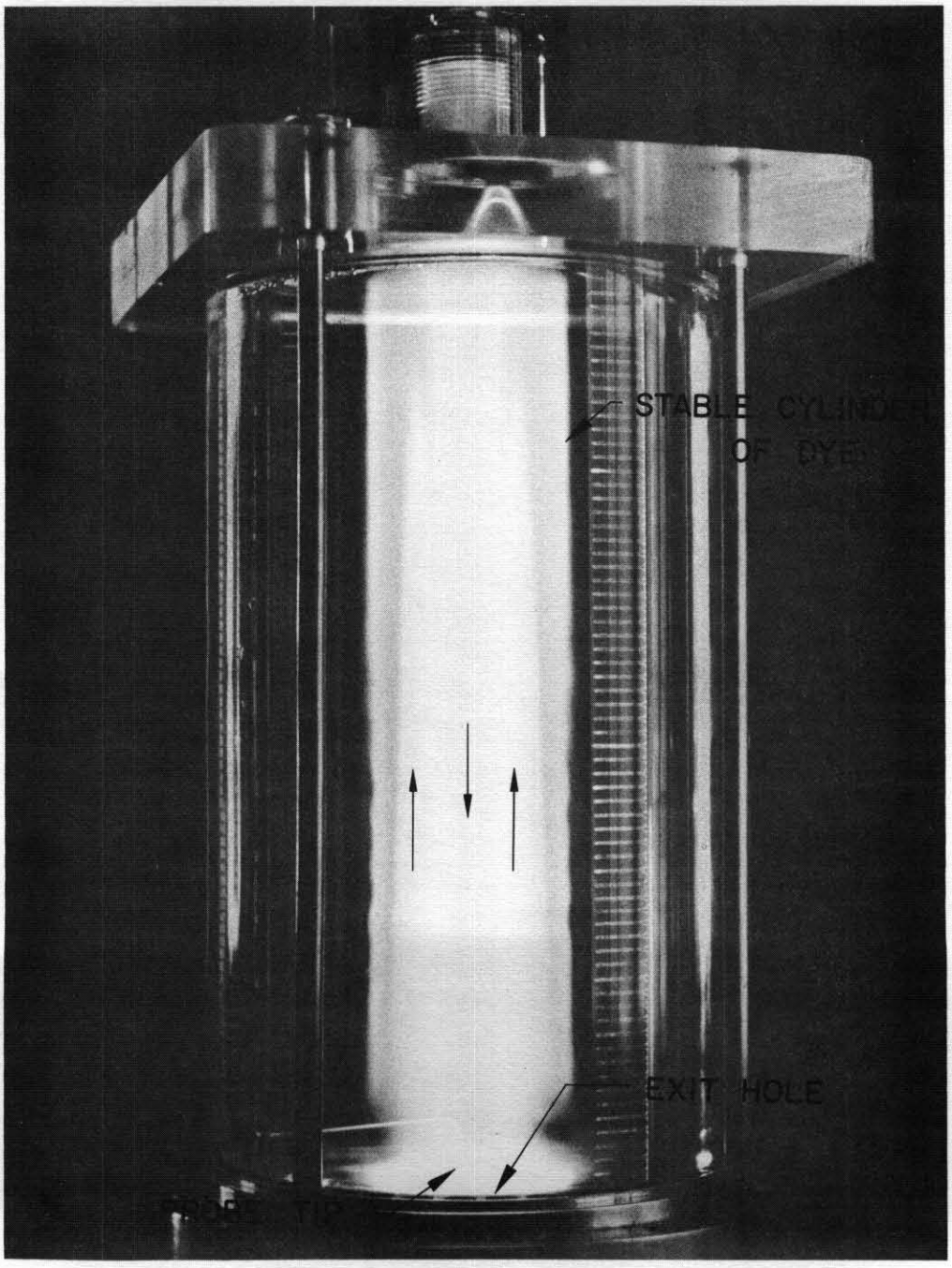

Fig. 21. Highly Curved End Wall. Secondary Flow Core within the Stable Core Shown in Figure 20

a recirculation region exists to some extent even for flat-end-wall cases. In the curved-end-wall case the larger boundary layer radial mass flow may induce a recirculation pattern strengthened sufficiently to produce observable modification of the inner vortex flow.

V. END-WALL INJECTION

In order to modify the secondary flow, and, if possible, to eliminate it, an end-wall slot injection system was constructed. The concept was motivated by consideration of the radial equilibrium within the end-wall boundary layer as discussed below.

The strong secondary flows in the vortex are a result of the large amount of radial mass flux within the boundary layer. This flux, in turn, is produced by the imbalance between the inward radial pressure gradient and the reduced centrifugal force field in the neighborhood of the wall (Fig. 1). If sufficient angular momentum can be imparted by tangential injection to overcome the velocity defect in this region then the secondary radial mass flow should be greatly reduced, or even virtually eliminated. In fact, if excess momentum be added in the neighborhood of the wall, it should be possible to reverse the direction of the radial flow within the boundary layer. This modification of the normal secondary-flow pattern was the goal of the end-wall injection configuration shown in Figs. 7, 8 and 9.

Assuming the validity of this concept, the question of how much mass flow would have to be injected to give the desired effect remained to be answered by experiment.

Figure 22 was made with 0 percent end-wall flow and discloses the strong upflow zone B emphasized by dye injected from a probe close to the lower end wall just outside the radius of the exit hole. A weak trace of the

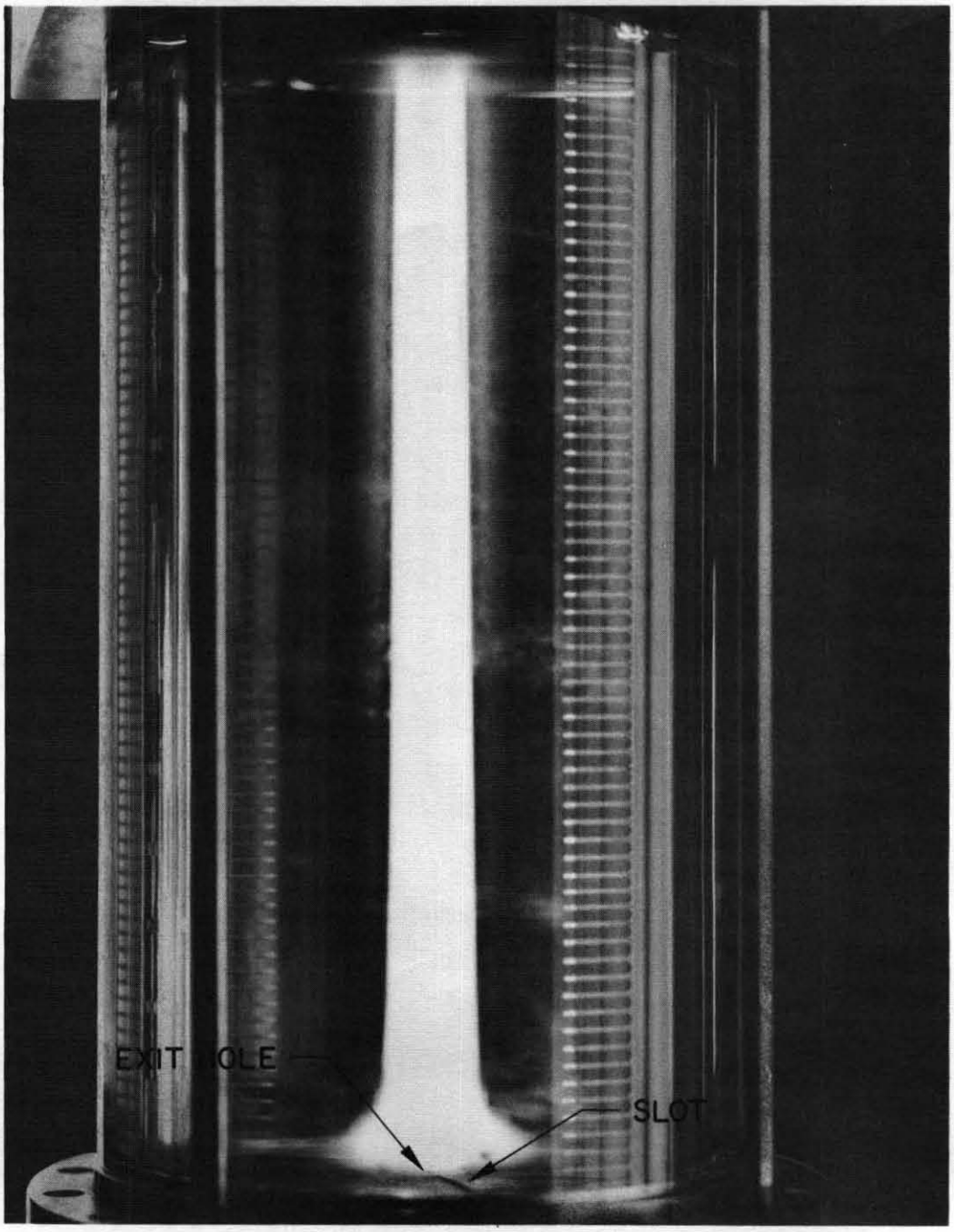

Fig. 22. End Wall Boundary Layer Slot Blowing Configuration. 0% End Wall Injection

downflow C region can also be seen just outside the B zone. Figure 23 shows the dramatic reduction in core strength resulting from 25 percent of the total mass flow directed through the slots in the upper and lower end walls; probe position and dye flow rate were identical to those of the previous figure. In Fig. 24 the core has virtually disappeared for an end wall flow fraction of 40 percent. The existence of a faint core can be attributed to the termination of the blowing slots at a radius somewhat greater than the exit hole, for constructional reasons.

The result of an even greater increase in the amount of end wall blowing can be seen in Fig. 25. Here 70 percent end-wall flow fraction has resulted in more tangential momentum added to the boundary layer region than that required to establish equilibrium. The excess centrifugal force results in radial outflow within the boundary layer and then helical flow along the side wall toward the vertical middle of the chamber. This flow was also influenced by the residual axial momentum in the slot jet flow. The secondary flow pattern has thus been completely altered.

With the initial four-slot end walls (Fig. 9a), substantial weakening of the core took place when 15 to 20 percent of the total mass flow was injected through the end wall slots (up to 10 percent at each end). Essential cancellation of the core was noted when about 45 to 50 percent of the total mass flow was diverted through the two end walls. Under the latter conditions the boundary layer streamlines were practically tangential, whereas without blowing, the streamlines spiralled steeply inward in a nearly radial direction.

An improved version of the end walls with narrower, contoured slots (Fig. 9b) resulted in a reduction of the amount of flow through the end walls required for core cancellation to a value of about 30 to 35 percent.

The foregoing results do not represent optimum or ultimate values by any means. Narrower slots or an alternate injection geometry giving higher

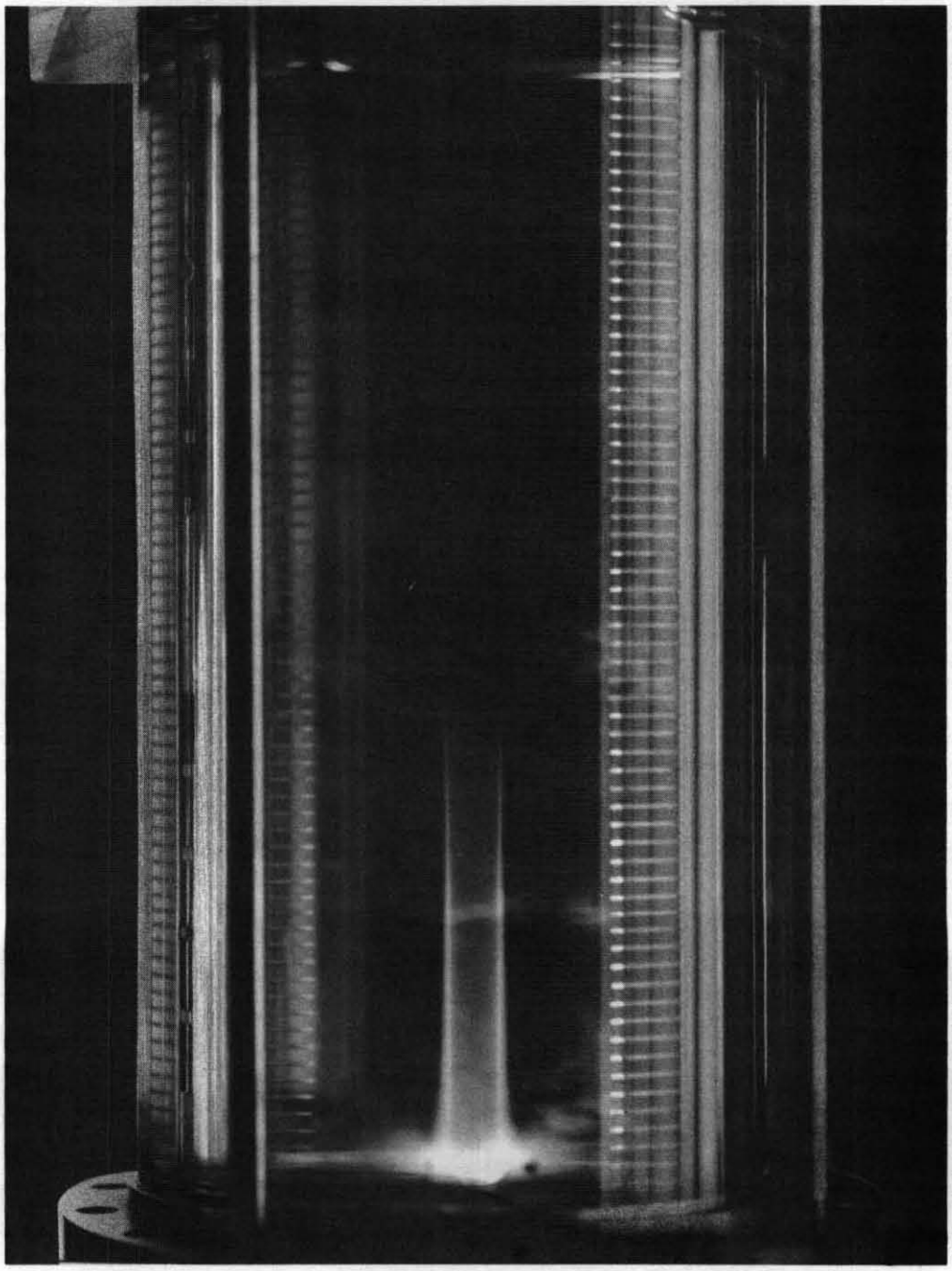

Fig. 23. End Wall Boundary Layer Slot Blowing Configuration. 25% End Wall Injection

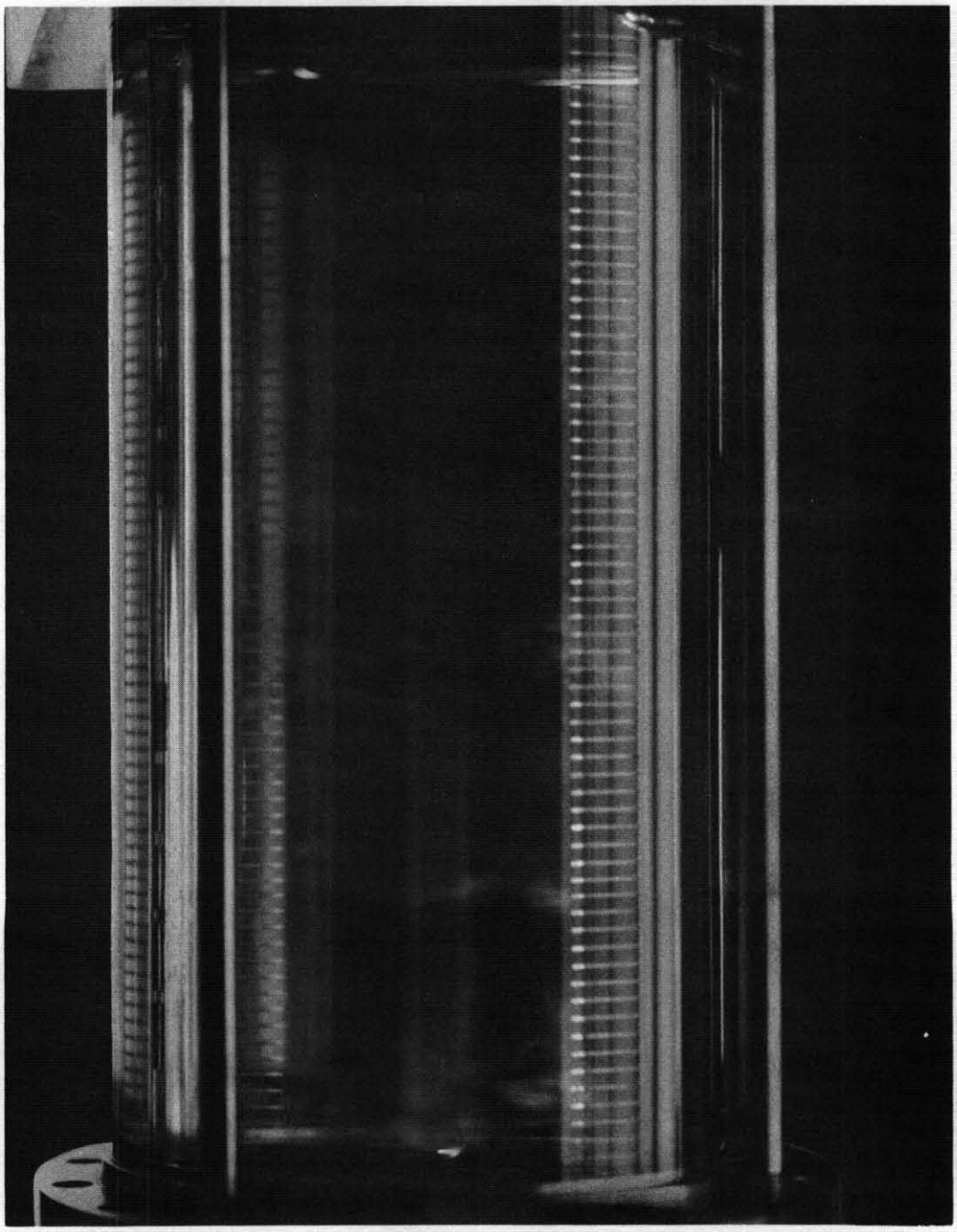

Fig. 24. End Wall Boundary Layer Blowing Configuration. 40% End Wall Injection

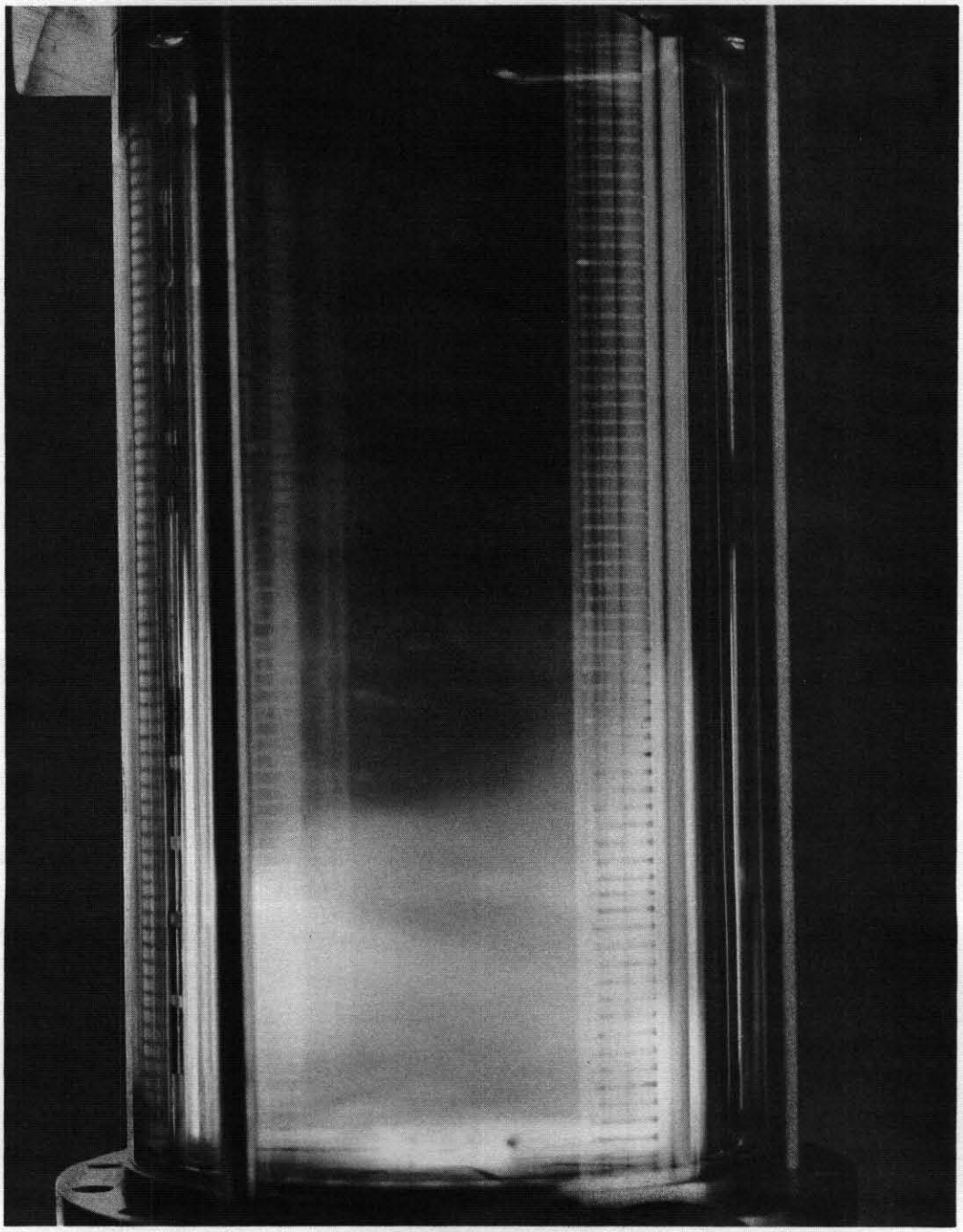

Fig. 25. End Wall Boundary Layer Blowing Configuration.
70% End Wall Injection

injection velocities (that is, a higher ratio of angular momentum to mass flow) together with detail improvements should result in substantial reduction in the mass flow required for core cancellation. By taking the ratio of the end-wall boundary-layer radial mass flow as given by Rott (Ref. 3) to the total chamber flow, it can be shown that this ratio is inversely proportional to the chamber length-to-diameter-ratio. From that result, it can be argued that the slot-injected mass flow fraction for secondary flow cancellation should also vary inversely with chamber length/diameter (L/D). Since the present experiment has an L/D of 3, reasonably small values of end-wall-injection mass-fraction should suppress secondary flows for an L/D of 10 or greater.

An alternate viewpoint in explaining the effects of end-wall blowing may be taken by considering the blown fluid as a rotating end wall, with a continuously varying angular velocity which increases from the outer wall toward the exit hole. The cause for this tangential velocity distribution is seen to be the radial distribution of static pressure within the vortex; the static pressure falls from the outer wall up to the vicinity of the exit hole radius and thus an end-wall-plenum pressure elevated slightly above the highest pressure within the vortex chamber will result in a pressure drop across the injection slots which increases radially inward. This situation produces a first-order match between the tangential velocity distributions of the vortex flow and the slot-blowing fluid. The previous argument tacitly assumes that the blowing mass flow is a reasonably small fraction of the total flow so that the side-wall driven vortex flow determines the chamber pressure distribution. If the major portion of the angular momentum entered the vortex chamber through end-wall injection, then the previous situation would be altered. End-wall injection of part of the chamber mass flow raises the problem of vortex driving efficiency; that is, the ratio of circulation in the vortex to the total enthalpy (or total pressure in the case of a water flow chamber) of the plenum fluid. The tangential injection of slot-blowing fluid does contribute to the vortex circulation. However, for

a given pressure drop the end-wall injection results in a lower circulation than side-wall injection since the fluid enters the chamber at a smaller radius. This effect should not be too serious if only a small fraction (for example, 10 to 20 percent) of the total flow need be injected through the end walls to overcome the local momentum defect. The afore-mentioned experiments have shown that a vortex can be driven by end-wall injection only, but this does not seem to be the optimum design for a vortex chamber.

VI. STEPPED END WALL

An end wall configuration having a deep, inward-facing step was used to explore the effect of a single large discontinuity upon the end-wall boundary layer and the secondary flow. It was hypothesized that such a step would result in substantial ejection of fluid from the end-wall boundary layer in the neighborhood of the step and that this ejection would in turn produce an annular zone of axial secondary flow. This was confirmed by experiment, with the modification that flow separation and re-attachment in a radial direction effectively broadened the sharpness of the discontinuity. The latter effect broadened the ejection zone and shifted it slightly inward.

The results from tests of the stepped end wall are shown in Figs. 26 to 29. In all cases Fluorescein dye was introduced through fine holes in the end wall to avoid possible disturbances from a probe placed close to the end wall. Figure 26 shows the annular core of axial flow produced just within the step radius; the latter can be seen at the lower end wall. In Fig. 27 an earlier stage in the axial growth of the dyed region is displayed, together with the faint outline of a previous dye pulse. The previously discussed A, B and C zones still exist in the region of the exit-hole, within the secondary flow zone produced by the step; dye injected near the exit-hole in Fig. 28 shows this clearly. Figure 29 was obtained by simultaneous dye injection

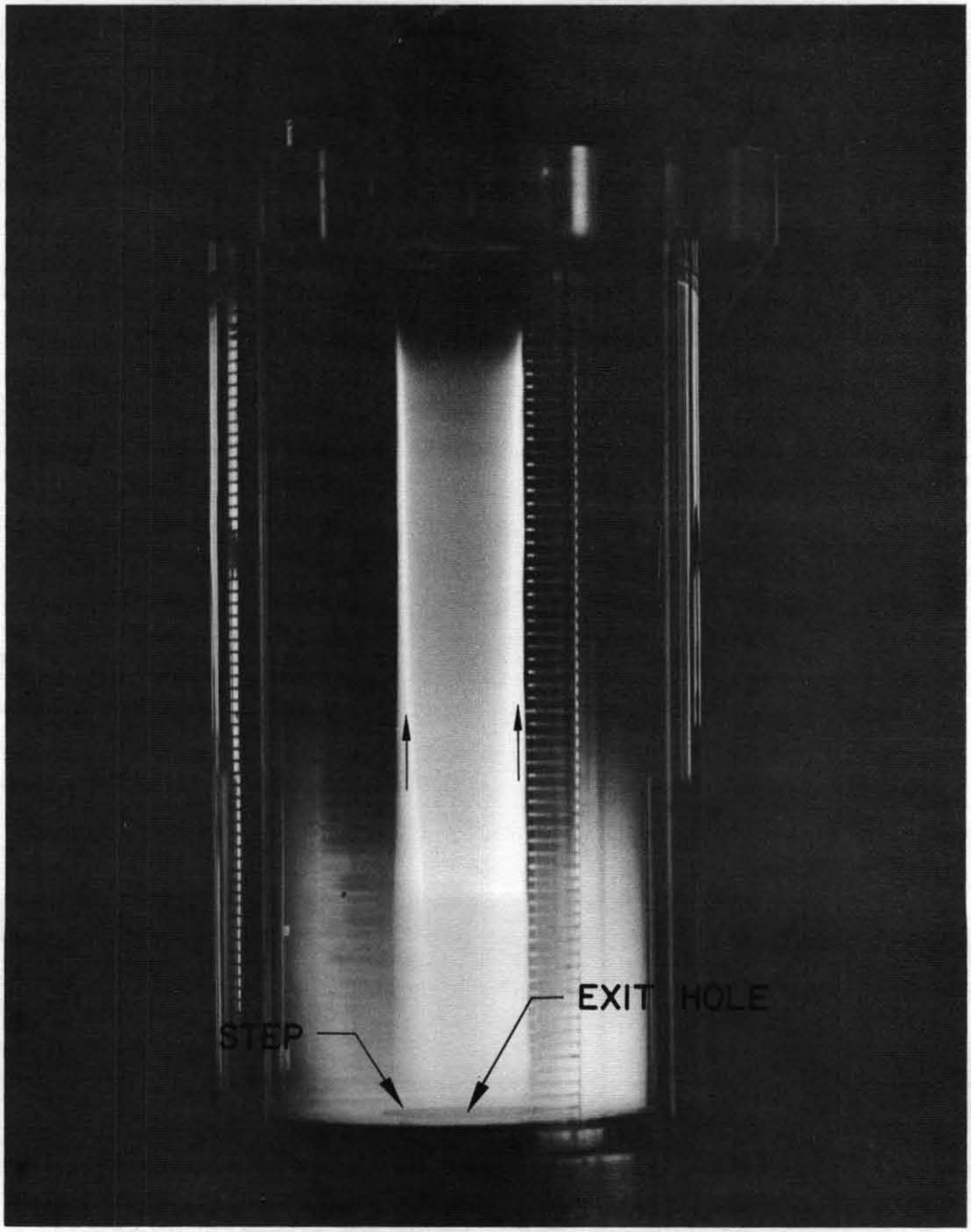

Fig. 26. Stepped End Wall. Cylindrical Zone of Fluid Injected from Boundary Layer at Step Is Shown

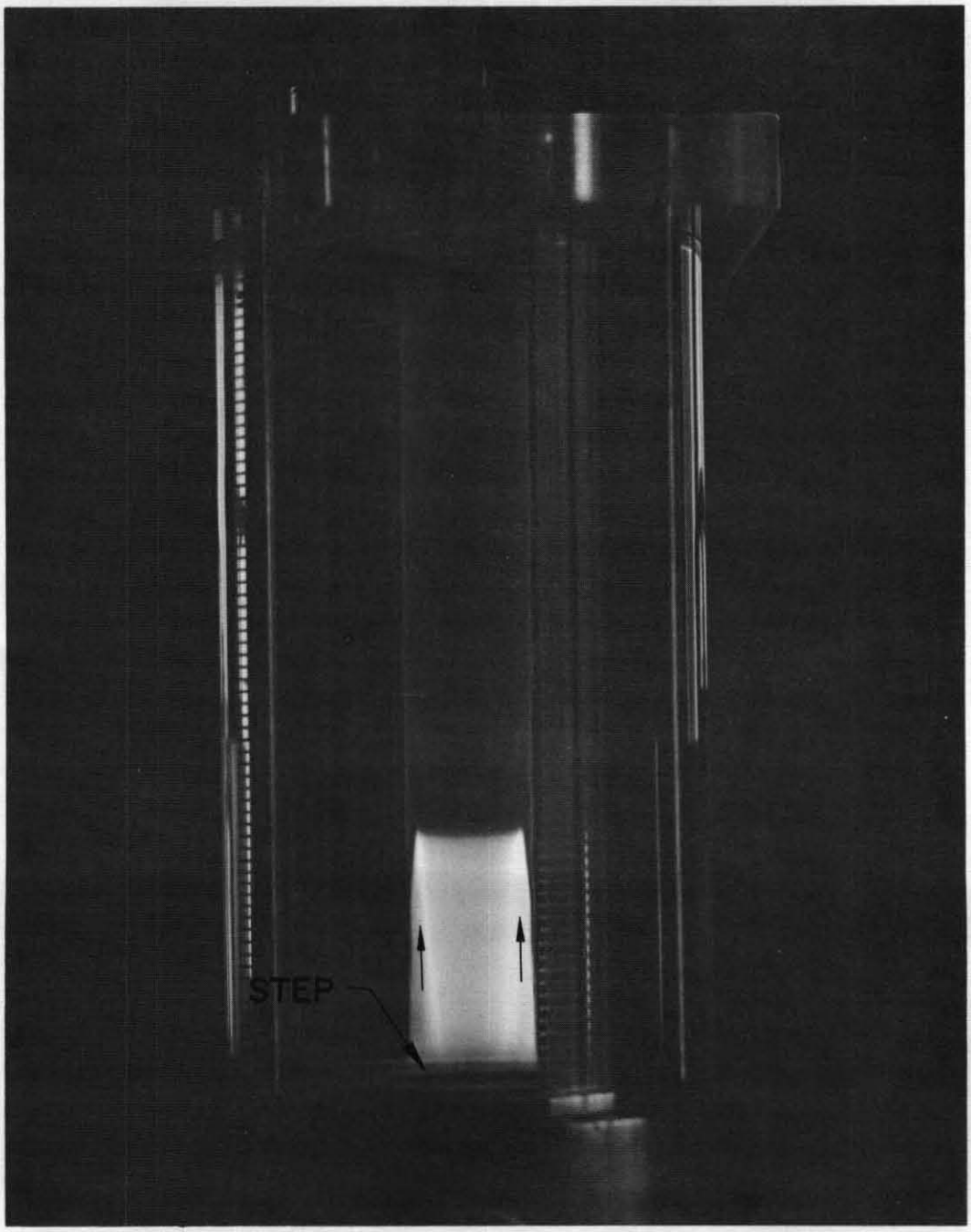

Fig. 27. Stepped End Wall. Faint Cylindrical Zone of Dye Remaining after 8 Minutes of Operation Together with New Pulse of Dye Emerging from Region of Step

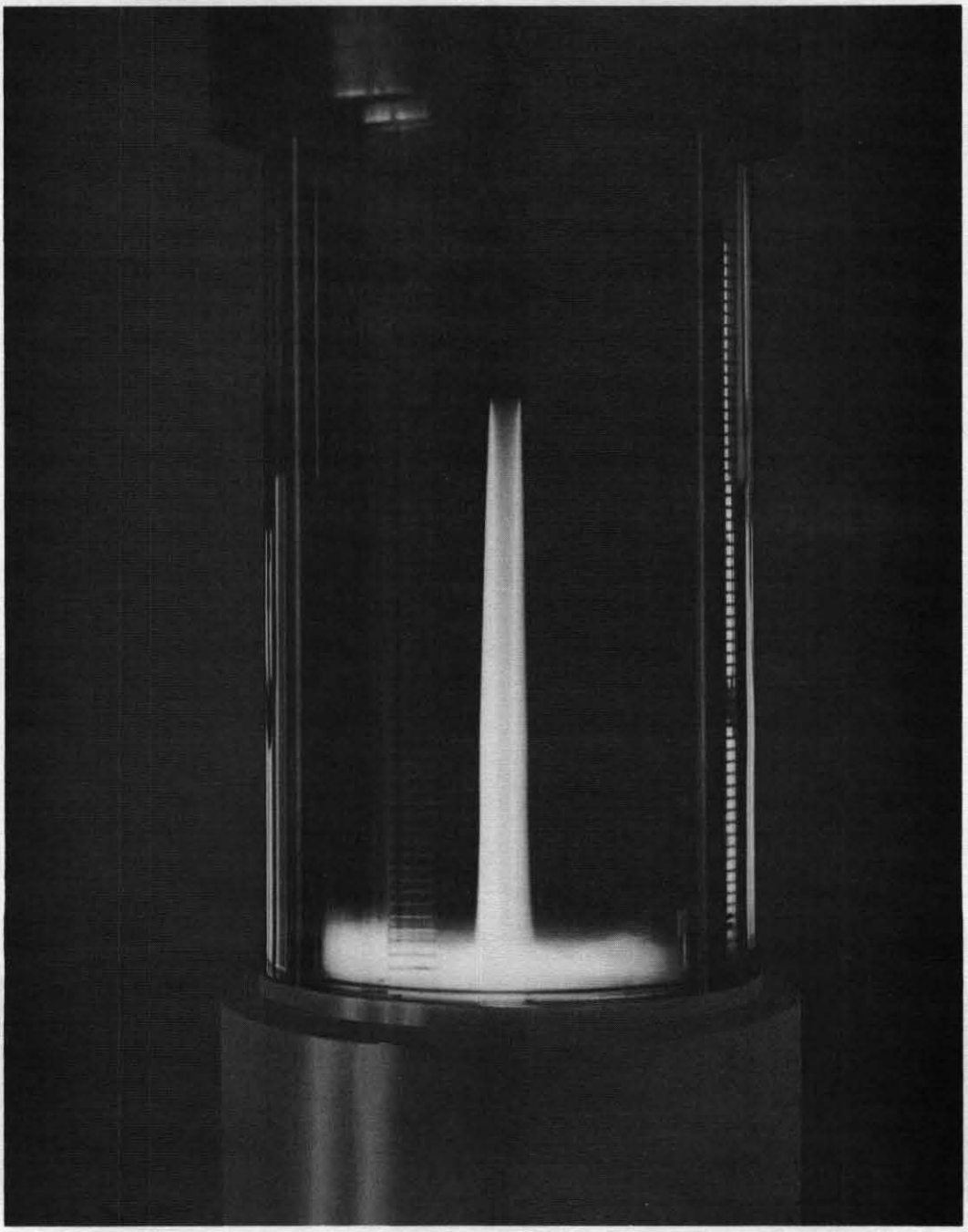

Fig. 28. Stepped End Wall Configuration Showing Ejection from Boundary Layer near Exit Hole within the Outer Ejection Zone Created by Step

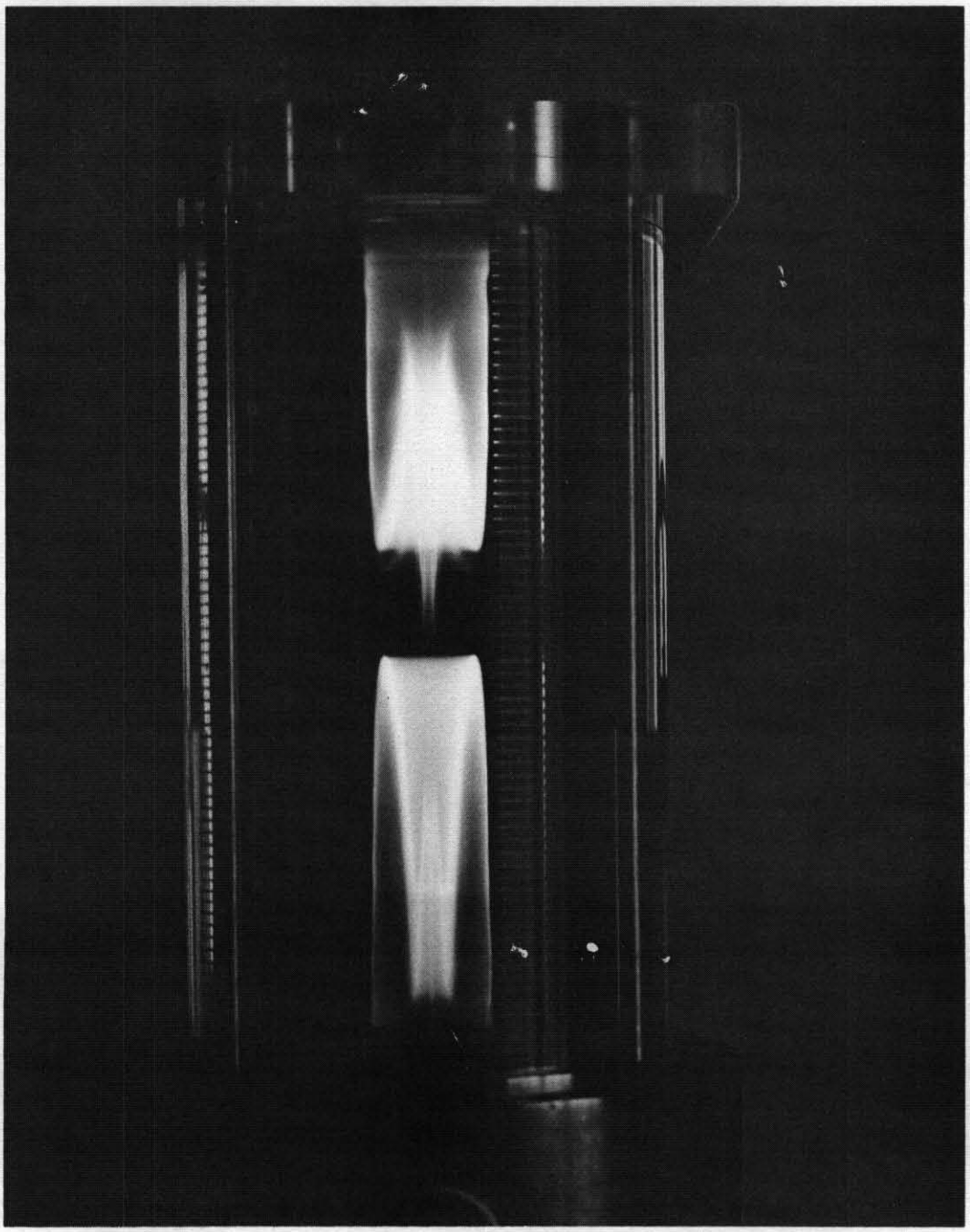

Fig. 29. Stepped End Wall. Dyed Zones of Fluid Ejected from Both End Wall Boundary Layers Showing Usual Multiple Zone Core Region Inside Step-Induced Zone

at each stepped end wall and the complicated pattern is a combination of the secondary flow regions resulting from both the exit hole and the step.

VII. CONCLUSIONS

The flow streamlines of enclosed jet-driven vortex flows are influenced by the secondary flows produced by viscous flow interactions.

Strong radial inflow occurs in the end-wall boundary layers under the influence of the vortex pressure gradient.

Fluid ejected from the end-wall boundary layers near the exit hole radius produces a central multiple-zoned core of axial secondary flow.

Fluid ejected from the boundary layer due to large discontinuities in the end-wall surface can also result in annular zones of axial flow.

Highly curved end walls apparently result in stronger radial flow in the boundary layer and a strong recirculation pattern within the chamber.

End-wall slot blowing can overcome the boundary layer radial inflow and consequently eliminate the central axial flow core. This tangential blowing was the only modification tried which had any appreciable effect on the core strength.

ACKNOWLEDGMENTS

The author expresses his appreciation for the many stimulating discussions with M. L. Rosenzweig and W. S. Lewellen and for the useful suggestions which resulted. Excellent technical support in construction and maintenance of the experimental equipment was provided by R. Cook and P. Amero. Among the support services of the Aerospace Corporation, particularly valuable assistance was provided by the still photo group (principally G. H. Moore) in recording flow patterns and the Laboratories Division Machine Shop in producing the intricate plexiglas parts.

REFERENCES

1. G. I. Taylor, "The Boundary Layer in the Converging Nozzle of a Swirl Atomizer", Quart. J. Mech. and Applied Mathematics, Vol. III, Part 2, 1950.

2. H. E. Weber, "Boundary Layer Inside a Conical Surface Due to Swirl", J. Applied Mech. 23, No. 4, December 1956.

3. N. Rott, "Turbulent Boundary Layer Development on the End Walls of a Vortex Chamber", Aerospace Corp. Report No. ATN-62(9202)-1, 30 July 1962.

4. J. M. Kendall, Jr., "Experimental Study of a Compressible Viscous Vortex", Jet Propulsion Laboratory Technical Report No. 32-290, June 5, 1962.

5. M. L. Rosenzweig, D. H. Ross, and W. S. Lewellen, "On Secondary Flows in Jet-Driven Tubes", J. Aerospace Sciences 29, No. 9, September 1962.

6. A. M. Binnie and J. D. Teare, "Experiments on the Flow of Swirling Water Through a Pressure Nozzle and an Open Trumpet", Proc. Royal Soc. A 235, pp 78-89, 1956.

7. J. L. Smith, Jr., "An Experimental Study of the Vortex in the Cyclone Separator", ASME Paper No. 61-WA-189 (1961).

8. J. F. Thompson, Jr., "The Structure of Free and Confined Turbulent Vortices" Research Report No. 44, May 1963, Aerophysics Dept., Mississippi State University.

9. W. S. Lewellen, "A Solution for Three-Dimensional Vortex Flows with Strong Circulation", J. Fluid Mech. 14, Part 3, pp 420-432, 1962.

10. M. L. Rosenzweig, W. S. Lewellen, and D. H. Ross, "Confined Vortex Flows with Boundary Layer Interaction", Aerospace Corp. Report ATN-64(9227)-2, 20 February 1964.

APPENDIX A. ANALYSIS OF NON-PLANAR END WALLS

The effect of non-planar end walls on the end-wall boundary layer mass flow is analyzed in an approximate manner by considering closed-form momentum integral solutions of the conical swirl flow problem. More general solutions involve extensive numerical computation and thus are not well suited to examination of trends. The aim of the analysis presented here is the determination of end-wall boundary layer radial mass flow as influenced by departure of the real wall surface from that of a flat plane disk perpendicular to the vortex axis. In spite of the approximations and simplified boundary conditions introduced, the results are deemed useful in estimating the effects of curved and conical end-walls.

Taylor (1950) solved a simplified formulation of the boundary layer flow over a converging conical surface with the main body flow consisting of a free-vortex tangential velocity distribution, together with radial and axial velocity components considered vanishingly small outside the boundary layer. The equations of motion for laminar flow are written in spherical polar coordinates and solved by a boundary layer momentum-integral technique. An arbitrary boundary layer velocity distribution and a single boundary layer thickness are assumed. In Taylor's notation the conical surface has a semi-vertex angle α, generator R_o, entrance (or large) radius R_3, orifice (small) radius R_2, and the circulation of the vortex is Ω. This geometry is displayed in Fig. 30. Non-dimensional boundary layer thickness δ_1 and radius R_1 are defined:

$$\delta_1 = \frac{\delta}{R_o}\left(\frac{\Omega}{\nu \sin \alpha}\right)^{1/2}$$

$$R_1 = \frac{R}{R_o}$$

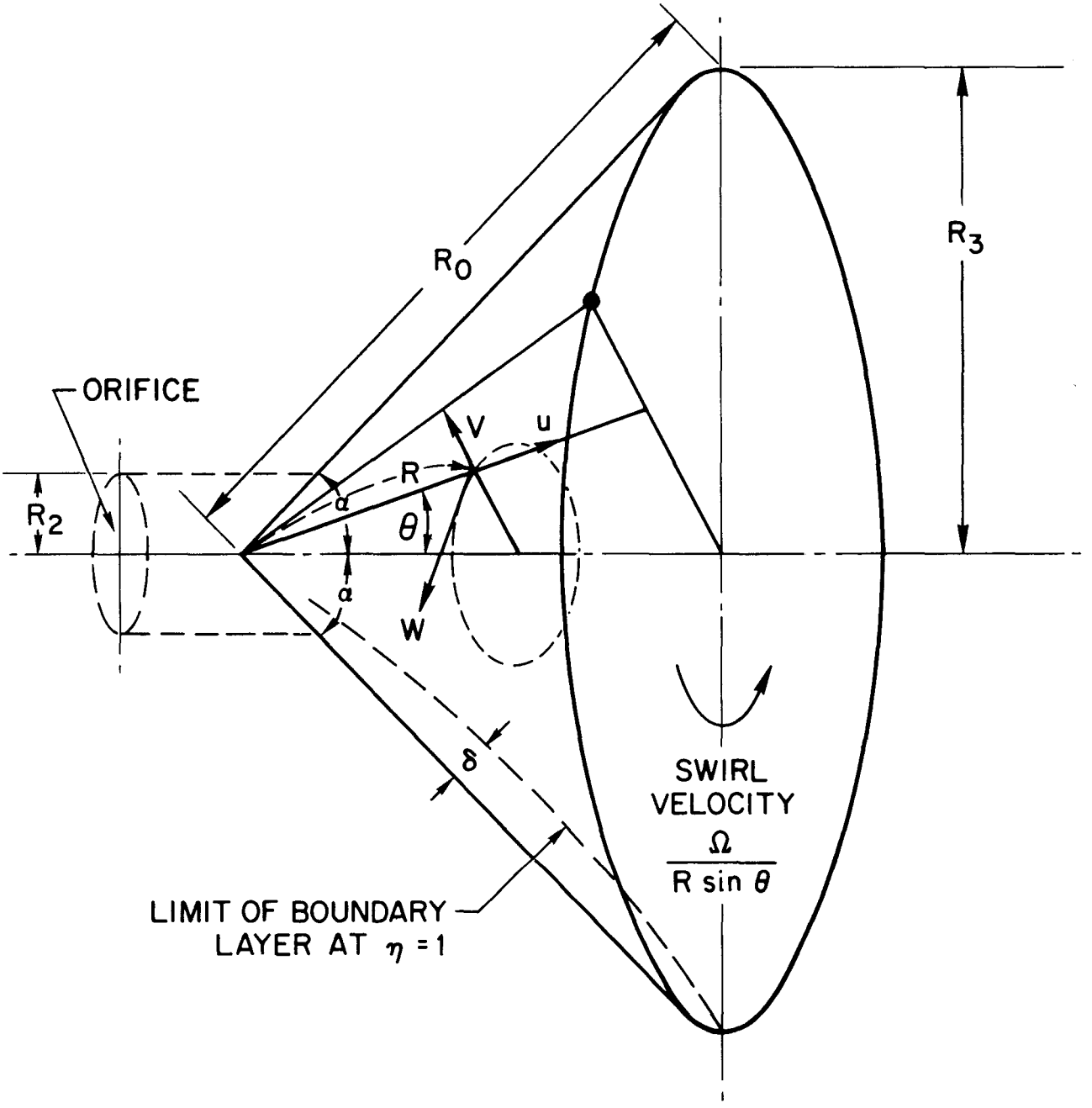

Fig. 30. Coordinates of Conical Swirl Flow in Notation of G. I. Taylor

where δ is the dimensional boundary layer thickness and ν the kinematic viscosity of the fluid. Another variable appears in the equations as

$$E = \frac{u}{w} \frac{\phi(\eta)}{f(\eta)}$$

E is thus a proportionality variable between the radial velocity u and the tangential velocity w in the boundary layer modified by the ratio of the tangential velocity distribution form function $\phi(\eta)$ to the radial form function $f(\eta)$. The term η is a dimensionless boundary layer position variable which varies from 0 at the surface to 1.0 at the outer edge.

Taylor's solution involves a numerical integration of his resultant ordinary differential equations giving E, δ_1, and χ (the angle between the flow streamlines at the surface and the conical generators) as universal functions of R_1. E and χ are related by

$$\cot \chi = \frac{1}{2} E$$

For the purpose of evaluating the effect of conical angle α on the boundary layer radial mass flow, it is noted that the latter quantity is the product of the actual boundary layer thickness δ times the average radial velocity

$$\overline{u} = \int_0^1 u \, d\eta$$

In the jet-driven vortex case the circulation Ω and inlet radius R_3 are given. Thus, $w = \Omega/R \sin \theta$ (θ is the angle a radius vector makes with the axis) is also given. Taylor's solution gives $E = E(R_1)$ and therefore $\overline{u} = \overline{u}(R_1)$. The functions $E(R_1)$ and $\overline{u}(R_1)$ are seen to be independent of α by definition. The term δ is the only dependent variable of R_1 which in turn depends upon α as a

parameter as seen from the definition of δ_1.

Now

$$\delta = \delta_1 R_o \left(\frac{\nu \sin a}{\Omega}\right)^{1/2}$$

and

$$R_3 = R_o \sin a$$

therefore

$$\delta = \delta_1 \frac{R_3}{\sin a} \left(\frac{\nu \sin a}{\Omega}\right)^{1/2}$$

$$= \left[\delta_1 R_3 \left(\frac{\nu}{\Omega}\right)^{1/2}\right] \left(\frac{1}{\sin a}\right)^{1/2}$$

$$= [\, g(R_1)] \left(\frac{1}{\sin a}\right)^{1/2}$$

The function $g(R_1)$ depends only upon given constants and R_1. Thus, for the case under consideration the boundary layer thickness δ and therefore the radial boundary layer mass flow varies as $(1/\sin a)^{1/2}$; resulting in a minimum value for the flat planar end wall, $a = \Pi/2$.

Weber (1956) extended the method of Taylor to the turbulent case by assuming a 1/7 power tangential velocity profile and a plausible radial profile. The classic pipe flow turbulent shear relation of Blasius is taken as valid for the more complex three-dimensional flow. The method is subject to the same simplifications and restrictions as Taylor's laminar case; in addition, the

shear stress relation and probably the profile distribution functions are more suspect. Therefore, the results should not be taken too literally but should serve as another general indicator for the end wall boundary layer behavior and also make an interesting comparison with the previously derived laminar results.

Since Weber's turbulent flow method is essentially that of Taylor with new assumptions about the specific form of the general profile parameters and shear stress term, it might be expected that the solution would have a general similarity in its functional form, but different numerical values. The results do show this behavior.

As in Taylor's case, the only term containing dependence upon α is the non-dimensional boundary layer thickness

$$\delta_1 = \frac{\delta}{R_o}\left(\frac{\Omega}{\nu \sin \alpha}\right)^{1/5}$$

where the new exponent 1/5 replaces the laminar value of 1/2. The basic assumptions for profile form parameters and shear stress are applied in each of these cases. Weber obtains a result which can be put into the form

$$\delta = [h(R_1)](\sin \alpha)^{-4/5}$$

where

$$h(R_1) = \delta_1 R_3 \left(\frac{\nu}{\Omega}\right)^{1/5}$$

This result has the same functional form as that for the laminar case, with different numerical values for the exponents. The flat planar end wall ($\alpha = \pi/2$) again gives the minimum mass flow.